Systematic proteomic profiling of the human Polycomb interactome

Simon Hauri[1,2,7*], Federico Comoglio[3,8*], Makiko Seimiya[3], Moritz Gerstung[3,9], Timo Glatter[1,10], Klaus Hansen[4], Ruedi Aebersold[1,5], Renato Paro[3,6], Matthias Gstaiger[1,2†] and Christian Beisel[3†]

1 Department of Biology, Institute of Molecular Systems Biology, ETH Zürich, Zürich, Switzerland
2 Competence Center Personalized Medicine UZH/ETH, Zürich, Switzerland
3 Department of Biosystems Science and Engineering, ETH Zürich, Basel, Switzerland
4 Biotech Research and Innovation Centre (BRIC) and Centre for Epigenetics, University of Copenhagen, Copenhagen, Denmark
5 Faculty of Science, University of Zürich, Zürich, Switzerland
6 Faculty of Sciences, University of Basel, Basel, Switzerland
7 Present address: Department of Clinical Sciences, Lund University, Lund, Sweden
8 Present address: Department of Haematology, Cambridge Institute for Medical Research and Wellcome Trust/MRC Cambridge Stem Cell Institute, University of Cambridge, Cambridge, United Kingdom
9 Present address: European Bioinformatics Institute (EMBL-EBI), Wellcome Genome Campus, Hinxton, United Kingdom
10 Present address: Mass spectrometry and proteomics, Max Planck Institute for Terrestrial Microbiology, Marburg, Germany

∗ Equal contribution
† Corresponding authors. M.G: matthias.gstaiger@imsb.biol.ethz.ch; C.B: christian.beisel@bsse.ethz.ch

Abstract

Polycomb group (PcG) proteins are major determinants of gene silencing and epigenetic memory in higher eukaryotes. Here, we used a robust affinity purification mass spectrometry (AP-MS) approach to systematically map the human PcG protein interactome, uncovering an unprecedented breadth of PcG complexes. The obtained high density protein interaction data identified new modes of combinatorial PcG complex formation with proteins previously not associated with the PcG system, thus providing new insights into their molecular function and recruitment mechanisms to target genes. Importantly, we identified two human PR-DUB de-ubiquitination complexes, which comprise the O-linked N-acetylglucosamine transferase OGT1 and a number of transcription factors. By further mapping chromatin binding of PR-DUB components genome-wide, we conclude that the human PR-DUB and PRC1 complexes bind distinct sets of target genes and impact on different cellular processes in mammals.

Introduction

Cell division requires faithful replication of the genome and restoration of specific chromatin states that form the basis of epigenetic memory[1]. Polycomb group (PcG)

proteins - originally identified in *Drosophila melanogaster* as epigenetic regulators stably maintaining the repressed state of homeotic genes throughout development - are key players in this process. Numerous studies have now established a central role for PcG proteins in the dynamic control of hundreds of targets in metazoans, including genes affiliated to fundamental signaling pathways[2]. Hence, biological processes regulated by PcG proteins encompass cell differentiation, tissue regeneration and cancer cell growth[3−5].

The PcG system is organized in multimeric repressive protein complexes containing distinct chromatin modifying activities, which impact on transcriptional regulation by modulating chromatin structures. In Drosophila, five distinct PcG complexes displaying different biochemical functions have been reported. The Polycomb Repressive Complex (PRC) 2 contains Enhancer of Zeste which trimethylates lysine 27 of histone H3 (H3K27me3)[6,7] while the PRC1 subunit Polycomb provides binding specificity to H3K27me3 through its chromo-domain[8,9]. In addition, PRC1 also contains the dRing protein, which catalyzes the mono-ubiquitination of histone H2A on lysine 118 (H2AUb1), thereby blocking RNA polymerase II activity[10−12]. The Pho (Pleiohomeotic, Drosophila homolog of mammalian YY1) repressive complex PhoRC combines DNA- and histone tail binding specificities[13], the PRC1-related dRing-associated factors complex dRAF contains the H3K36-specific histone demethylase dKDM2[14] and the Polycomb repressive deubiquitinase (PR-DUB) targets H2AUb1[15].

Although the core components of Drosophila PcG complexes seem rather fixed, we and others have shown that they can be co-purified with different sets of accessory proteins, thus increasing the diversity of the PcG system[13,16−18]. Epigenomic profiling revealed that distinct PcG complexes target largely overlapping gene sets in Drosophila and mechanistic details of PcG recruitment to target genes are beginning to emerge[15,19−22].

In contrast, the mammalian PcG system is less well defined and appears to be significantly more complex. Each Drosophila PcG subunit has up to six human homologs, which combinatorially assemble in different complexes[23−26]. The six homologs of the Drosophila PRC1 core protein Psc, PCGF1-6, purify together with RING2, the homolog of dRing, in different complexes named PRC1.1-PRC1.6, and each of them associates with specific additional components[23−27]. These PRC1 complexes are further distinguished by the mutually exclusive presence of RYBP or a chromo-domain containing CBX protein. Five different CBX proteins displaying differential affinities for lysine-methylated histone H3 tails and RNA[28] have been linked to PRC1. In contrast, the absence of a chromo-domain within RYBP suggests that recruitment of CBX and RYBP containing PRC1 complexes might be mediated by H3K27 methylation or be independent of it, respectively. Indeed, recent work showed that the histone demethylase Kdm2b targets PRC1.1 via direct binding to unmethylated CpG islands[29−31]. Interestingly, incorporation of RING2 in optional PCGF complexes not only leads to differential recruitment to chromatin but also differentially regulates its enzymatic activity[23,29,31−34].

Similarly to PRC1, the histone methyltransferase (HMT) activity of PRC2 is potentially modulated by accessory components such as the Polycomb-like homologs PHF1, PHF19 and MTF2[35−36]. Additional DNA binding interaction partners like JARD2 and AEBP2 might mediate recruitment of the complexes to chromatin[37−41]. However, whether the PRC2 core, consisting of EED, SUZ12 and EZH2, simultaneously interacts with all of these components or whether distinct complexes co-exist remains unknown. Moreover, mammalian PhoRC and PR-DUB have not been identified to date.

Understanding PcG-mediated epigenetic regulation in mammals requires a detailed understanding of the dynamic assembly of PcG complexes. A required step towards this goal is the exhaustive definition of the composition of individual PcG complexes including all accessory proteins, which likely convey distinct functional effects. Here we present the first systematic and comprehensive high-density map on the modular

organization of the human PcG system using a sensitive double-affinity purification and mass-spectrometry (AP-MS) method[42−43]. The refined map of 1400 interactions and 490 proteins led to a considerable refinement of the human PRC1 and PRC2 network topology, including their relation with the heterochromatin silencing system and the identification of several novel interaction partners. Furthermore, we determined the composition of the human PR-DUB. We found that this highly diverse complex contains MBD proteins, FOXK transcription factors and OGT1, an O-linked N-acetylglucosamine (O-GlcNAC) transferase implicated in PcG silencing in Drosophila[44]. Finally, chromatin profiling of PR-DUB components and comparison with published chromatin maps of PcG proteins indicates that as opposed to Drosophila, PRC1 and PR-DUB regulate distinct sets of genes in human cells.

Results and Discussion

Systematic mapping of the human PcG interaction proteome

To investigate the human PcG protein interaction network, we applied a systematic proteomics approach, based on our previously reported AP-MS protocol in HEK293 cells[42]. The method employs Flp-In HEK293 stable cell lines expressing Strep-HA tag fusion proteins upon tetracycline induction (Fig. 1a). Initially, we selected 28 PcG proteins homologous to Drosophila core complex components and performed AP-MS experiments using these proteins as *primary baits* (Supplementary Fig. 1a). Then, based on the observed interaction data from this set, we chose 36 additional *secondary bait* proteins (Supplementary Fig. 1a, Supplementary Table 1). After double affinity purification, bait-associated proteins (preys) were identified by liquid chromatography tandem mass spectrometry (LC-MS/MS; Fig. 1a).

At least two biological replicates were measured for each bait protein, for a total of 174 AP-MS measurements. Proteins were identified using the X!Tandem search tool to match mass spectra to peptides, and the Trans-Proteomic Pipeline (TPP) to map peptides to proteins, at a false discovery rate (FDR) of less than 1%[45,46]. The resulting raw data set contained 930 proteins exhibiting 9856 candidate interactions.

To efficiently discriminate biologically relevant interaction partners from contaminant proteins, we devised a stringent filtering procedure based on both WDN-score[47] and average enrichment over control purifications for each bait-prey pair. This filtering strategy retained 490 high confidence interacting proteins (HCIPs) encompassing 1400 (1193 unidirectional and 207 reciprocal) interactions. Our data set is characterized by an average of 21.9 HCIPs per bait protein, with 75% of interactions that have not yet been annotated in public databases (Supplementary Fig. 1b).

To evaluate the specificity and sensitivity of our AP-MS data, we considered the two bait proteins exhibiting the highest number of HCIPs, SKP1 (79 HCIPs) and WDR5 (73), and performed a cross-validation with literature-based reports. SKP1 serves as an adaptor for F-Box proteins and CUL1, and confers enzymatic specificity. Out of 79 HCIPs, our SKP1 purifications identified 42 F-Box proteins (Supplementary Fig. 1c). Furthermore, a previous AP-MS study investigating the interaction partners of WDR5[48] identified a set of 21 proteins associating with this scaffold protein, which takes part in the assembly of several chromatin regulating complexes (reviewed in Migliori et al.[49]). Notably, while we were able to recall 76% of previously reported interaction partners, our experiments identified an additional set of 48 proteins (Supplementary Fig. 1d) co-purifying with WDR5 and encompassing MLL complexes, the NSL complex, the ADA2/GCN5/ADA3 transcription activator complex, mTORC2 components RICTOR and SIN1, and the Polycomb repressive complex PRC1.6 (Supplementary Fig. 1e).

Hierarchical clustering assigns HCIPs to PcG complexes

To determine the topology of our protein interaction network, we performed hierarchical clustering of HCIPs using a rank-based correlation dissimilarity measure (see Supplementary Methods for details). Clustering revealed a modular organization built upon the three major PcG assemblies PRC1, PRC2 and PR-DUB, and HP1-associated complexes (Fig. 1b-c).

PRC1 represents the most elaborated and heterogeneous assembly, containing four groups of complexes defined by the six PCGF proteins: PRC1.1 (PCGF1), PRC1.2/PRC1.4 (PCGF2/4), PRC1.3/PRC1.5 (PCGF3/5) and PRC1.6 (PCGF6). Among these PRC1 assemblies, PRC1.6 further provides links to the heterochromatin control system via the HP1 chromobox proteins CBX1 and CBX3. Although analysis of the PRC1 topology has been recently reported in studies concentrating on specific subunits in various cellular systems[23,50−52] our systematic high-density interaction data allowed us to further refine the composition of the PRC1 module. In the following discussion we focus on these novel findings regarding PRC1 organization, which is illustrated in Fig. 1b-e and Supplementary Fig. 3, and detailed in Supplementary Table 2.

All four PRC1 assemblies share a common core encompassing the E3 ubiquitin ligases RING1 and RING2, and - with exception of PRC1.2/PRC1.4 - RYBP and YAF2. Interestingly, PCGF2/4 also interact with RYBP and YAF2. As these proteins do not share any additional interaction partner besides RING1/2 (Supplementary Fig. 3b), RYBP/YAF-PCGF2/4-RING complexes might have limited functionality compared to other PRC1 complexes or correspond to transient products before specific canonical and non-canonical PRC1 holo complexes assemble. Furthermore, we did not detect any protein stably associating with all canonical PRC1 core members (RING1/2, PHC1-3, CBX2/4/6/7/8, PCGF2/4). However, we identified NUFP2 (Nuclear fragile X mental retardation interacting protein 2), a putative RNA binding protein exhibiting interactions with CBX2/6/7, PHC3 and PCGF4, as a new PRC1 interacting protein (Supplementary Fig. 3b).

The PRC2 complex is separated from both PRC1 and HP1 (Fig. 1c). The two characteristic histone binding proteins RBBP4 and RBBP7 not only belong to the PRC2 core along with SUZ12, EED and EZH1/2, but also partake in other protein complexes such as LINC, NURF, NURD and SIN3 (Supplementary Fig. 2a).

Finally, we identified the PcG complex PR-DUB defined by ASXL1/2 and BAP1 (Fig. 1c). Our clustering analysis also revealed complexes such as the TCP chaperonin and the proteasomal lid, that primarily consist of prey proteins (Fig. 1b). Of note, several proteins belonging to MLL complexes share interactions between PRC1.3/PRC1.5 (CSK21/22), PRC1.6 (WDR5) and PR-DUB (OGT1) (Fig. 1c). In contrast, interaction modules centered on LMBL1/3/4, SUV92 and TRIPC, LCOR, ZN211, and YY1 (the homolog of Drosophila Pho) are more disconnected and tend to be sparse (Fig. 1c, Fig. 2d and Supplementary Fig. 2b-c). Although YY1 interacts with all subunits of the INO80 chromatin remodeling complex, our AP-MS data does not unveil an equivalent of the Drosophila PhoRC complex (Supplementary Fig. 2b). However, except for PhoRC, we were able to reconstitute all mammalian equivalents of Drosophila PcG protein assemblies with unprecedented detail.

WD40 domain proteins DCAF7 and WDR5 are central scaffolding proteins for PRC1.3/PRC1.5 and PRC1.6

The WD40 domain protein DCAF7 has been implicated in skin development and cell proliferation by interacting with DIAP1 and the dual-specificity tyrosine phosphorylation-regulated kinase DYR1A[53,54]. Intriguingly, DCAF7 co-purified with CBX4/6/8, RING1/2, RYBP/YAF2 and PCGF3/5/6, indicating that the protein is deeply embedded in the

PRC1 module. As recent studies also reported interactions between DCAF7 and members of the canonical PRC1 complex, as well as PCGF3/5/6[26,27,55,56], we performed DCAF7 purifications to test whether the protein is indeed a universal subunit of several different RING1/2-containing complexes.

Our DCAF7 AP-MS revealed reciprocal interactions with all bait proteins within a cluster centered on PCGF3 and 5 (Fig. 1d and Supplementary Fig. 3c), with no relation to the other PCGF complexes. Moreover, we identified DYR1A/B, DIAP1, the Zinc finger transcription factors (ZNFs) ZN503 and ZN703, and the ankyrin-repeat proteins SWAHA and SWAHC as an unrelated module interacting with DCAF7 (Fig. 1d). This result suggests that DCAF7 acts as a scaffold for several different protein complexes.

As for RING1/2, RYBP/YAF2 and PCGF3/5, DCAF7 interacts with the tetrameric casein kinase 2 (CSK2) and the three paralogs AUTS2, FBRS and FBSL. Therefore, to further refine the PRC1.3/PRC1.5 sub-network we performed AP-MS experiments using the catalytic casein kinase subunits CSK21 and CSK22. Our results confirmed the topology of the PCGF3/5-DCAF7 assemblies, and identify CSK2 and three uncharacterized proteins within the AUTS2 family as part of PRC1.3/PRC1.5 (Fig. 1d and Supplementary Fig. 3c).

The protein PCGF6 was initially purified together with the transcription factors E2F6, MAX, TFDP1, MGAP as well as RING1/2, YAF2, LMBL2, CBX3 and the HMTs EHMT1 and EHMT2, an assembly denoted as E2F6.com[57]. However, subsequent studies were unable to recover the entire (holo) E2F6.com[23,27,58,59]. Moreover, recent data suggest that PCGF6 and RING2 might interact with the WD40 domain protein WDR5[23]. We therefore decided to revisit the topology of the PCGF6-E2F6 network and to probe WDR5 connectivity by adding MAX, TFDP1, E2F6, LMBL2, CBX3, EHMT2 and WDR5 to our bait collection. Our AP-MS experiments unraveled a high-density network including reciprocal interactions between all but one (EHMT2) baits within this set (Fig. 1e and Supplementary Fig. 2c), thus demonstrating that the major PRC1.6 complex resembles E2F6.com. In addition, MGAP, MAX, TFDP1 and E2F6 purifications revealed a rich set of transcription factors that can heterodimerize with these proteins but that are not part of PRC1.6 as they did not connect to any other component thereof (Fig. 1e).

Recently, WDR5 was also reported to be part of the Non-Specific Lethal (NSL) complex and to form a trimeric complex with RBBP5 and ASH2L, which stimulates the H3K4-specific activity of the SET1 HMT family members SET1A, SET1B and MLL1-4[48,60−62]. Interestingly, while we recalled these interactions, we additionally detected reciprocal interactions of WDR5 with all PRC1.6 subunits, thus demonstrating that WDR5 is a universal component of activating and repressing chromatin modifying complexes.

Taken together, our results identify the WD40 domain proteins DCAF7 and WDR5 as subunits of PRC1.3/PRC1.5 and PRC1.6, respectively. Importantly, recent studies suggested that the diversity of PRC1 complexes might be specified by binding preferences of PCGF proteins, which are mediated by their RING finger- and WD40-associated Ubiquitin-Like (RAWUL) C-terminal domain[63,64]. For example, the PCGF1 and PCGF2/4 RAWUL domains selectively interact with BCOR/BCORL and PHC proteins, respectively[63]. Since no interaction partners of PCGF3/5 and PCGF6 RAWUL domains have been experimentally identified to date, and since WD40 domain-containing proteins often scaffold multisubunit complexes[49], we propose that DCAF7 and WDR5 may serve as central scaffolding proteins for PRC1.3/PRC1.5 and PRC1.6.

CBX1 partitions in several distinct heterochromatin complexes including PRC1.6

In contrast to previous studies, which reported CBX3 as the only heterochromatin protein within E2F6.com, we unexpectedly detected CBX1 in all our PRC1.6-related pull down experiments. To corroborate this finding, we performed AP-MS experiments with CBX1, using the constitutive heterochromatin protein CBX5 as control. Our results indicate that while CBX5 is disconnected from the PCGF6-E2F6 network, components therein interact with CBX1 (Fig. 1e and Supplementary Table 2). Furthermore, they validate interactions of EHMT2 with CBX1 and CBX3 and, to our surprise, separate EHMT2 and EHMT1 from PRC1.6, suggesting a separate complex containing CBX1/3, EHMT1/2, ZNF proteins, as well as the KRAB-ZNF interacting and co-repressor protein TIF1B (Supplementary Fig. 4a).

Since the PcG and heterochromatin silencing systems are functionally and molecularly related through PcG CBX2/4/6/7/8 and HP1 CBX1/3/5 proteins (reviewed in Beisel and Paro[65]), we further explored the CBX1/3/5 core of our network seeking for potential connections between these two systems. This survey led to a refined topology of CBX1/3/5-containing complexes and identified new interacting partners (Supplementary Fig. 4b-e). However, we did not detect additional connections to PcG proteins, suggesting limited direct cross-talk between protein components of the two silencing systems.

The PRC2 core partitions into two different classes of complexes

While the functional core complex of PRC2 is composed of SUZ12, EED, RBBP4/7 and either EZH1 or EZH2, additional accessory proteins have been identified which may regulate the H3K27 HMT activity of the complex and its recruitment to chromatin[66−68]. However, how these proteins are organized within PRC2 or whether they assemble into independent PRC2 subcomplexes remains largely unresolved. To elucidate the topological organization of PRC2 complexes we performed AP-MS experiments using 14 reported PRC2-associated proteins (Supplementary Fig. 1a).

Hierarchical clustering analysis assigned all PRC2 baits to a single cluster exhibiting high intra-cluster correlations (Fig. 1b and 2a) and forming a high-density interaction network (Fig. 2b). However, when reciprocal interactions were taken into account, our data revealed two fundamental alternative assemblies linked to the PRC2 core, the first defined by AEBP2 and JARD2 and the second by the mutually exclusive binding of one of the three Polycomb-like homologs (PCLs) PHF1, PHF19 and MTF2, respectively (Fig. 2b).

Taken together, our results identify two structurally distinct classes of PRC2 complexes. We therefore propose a novel nomenclature for PRC2, in which we refer to the two PRC2 wings as PRC2.1 (mutually exclusive interaction of PHF1, MTF2 or PHF19) and PRC2.2 (simultaneous interaction of AEBP2 and JARD2). AEBP2 and JARD2 can directly bind to DNA and have been implicated in the recruitment of PRC2 and modulation of its enzymatic activity[37−39,67]. Interestingly, depletion of JARD2 has only a mild effect on global H3K27 methylation levels, suggesting that PRC2.1 might be primarily responsible for maintaining H3K27me3 patterns genome-wide.

C10ORF12 and C17ORF96 are mutually exclusive subunits of the Polycomb-like class of PRC2 complexes

Our purifications of the PRC2 core members and PCLs identified two largely uncharacterized proteins, C10ORF12/LCOR and C17ORF96, as PRC2 interactors (Fig. 2b). Both proteins have recently been shown to reciprocally interact and co-localize on chromatin

with EZH2[66], but their placement within the PRC2 topology and their functional role remained unknown.

Purifications of C17ORF96 confirmed all interactions with PCLs (Fig. 2b) and computational sequence analysis revealed that C17ORF96 is present in all vertebrate genomes. Interestingly, BLAST identified a single protein related to C17ORF96 in the human genome, the SKI/DAC domain containing protein 1 (SKDA1) (Supplementary Fig. 5a). SKDA1 belongs to the DACH family, which is defined by the presence of a SKI/SNO/DAC domain of about 100 amino acids, and is involved in various aspects of cell proliferation and differentiation[69,70]. However, C17ORF96 lacks the SKI/SNO/DAC domain and its homology to SKDA1 is restricted to the C-terminus (53% sequence identity within the last 60 amino acids) (Supplementary Fig. 5a-b), suggesting that this region encodes an hitherto uncharacterized protein domain. Interestingly, SKDA1 also interacts with EZH1 and SUZ12 (Fig. 2b), suggesting that this putative C-terminal domain mediates the interaction of C17ORF96 and SKDA1 with the PRC2 core.

Initial analysis of C10ORF12, the second uncharacterized protein highly connected to the PRC2 core, identified peptides that ambiguously mapped to two distinct UniProt proteins, LCOR and C10ORF12 (Supplementary Fig. 5c-e). These two proteins are encoded by the same genomic locus. Indeed, in contrast to the UniProt database, Genebank contains the LCOR-Cra_b (ligand-dependent co-repressor, isoform CRA_b, EAW49962.1) entry, where the N-terminal 111 amino acids of LCOR are fused to C10ORF12 and the two regions are separated by a 200 amino acid spacer (Fig. 2c). LCOR is a ligand-dependent co-repressor interacting via its N-terminal domain with nuclear hormone receptors in a complex including CTBP and a number of histone deacetylases[71,72]. While our AP-MS analysis yielded peptides of the LCOR N-terminus, C10ORF12 and the LCOR-CRA_b specific spacer (Supplementary Fig. 5c), peptides of the LCOR C-terminus were missing (Supplementary Fig. 5d), indicating that PRC2 interacts with LCOR-CRA_b and potentially with the shorter isoform C10ORF12. To test this possibility, we performed additional AP-MS experiments using LCOR, C10ORF12 and LCOR-CRA_b as baits. LCOR purified with its known interaction partners CTBP1 and CTBP2, while PRC2 components were absent in LCOR purifications (Fig. 2d and Supplementary Fig. 5e). In contrast, both LCOR-CRA_b and C10ORF12 reciprocally interact with all subunits of the PCL wing of PRC2 (Fig. 2b, Supplementary Fig. 5d-e).

To investigate the functional relevance of this finding, we employed a heterologous reporter system based on a stably integrated, constitutively active luciferase reporter gene responsive to upstream, promoter-proximal GAL4 DNA binding sites (Fig. 2e)[73]. We engineered cell lines containing tetracycline inducible GAL4-LCOR and GAL4-C10ORF12 expression constructs, respectively. Upon induction, both proteins accumulated in the nucleus and were recruited to the GAL4 motifs, resulting in strong repression of luciferase activity (Fig. 2f-h and Supplementary Fig. 5f). To assess whether the repressive activity of C10ORF12 is mediated by recruitment of PRC2 to the target promoter, we performed chromatin immunoprecipitation (ChIP) with an H3K27me3-specific antibody and analyzed the enrichment of luciferase promoter fragments via quantitative PCR. Upon tetracycline induction, we found that the transcription start site (TSS) of the luciferase gene was significantly trimethylated at H3K27 in the GAL4-C10ORF12 expressing cell line (Fig. 2i). In contrast, despite GAL4-LCOR was expressed at higher levels than GAL4-C10ORF12 (Fig. 2f) and exhibited a 10-20 fold increase in its binding to the reporter (Fig. 2h), no significant H3K27me3 enrichment was observed upon expression of this protein.

PCL proteins target PRC2 and positively regulate its enzymatic activity via their ability to bind methylated H3K36[36,74,75]. However, further experimental investigation will be required to elucidate the exact mechanism by which C17ORF96 and LCOR-CRA_b/C10ORF12 influence PRC2.1. An interesting possibility is that LCOR-CRA_b

recruits PRC2.1 to nuclear hormone receptor binding sites upon ligand binding. This interaction, restricted to C10ORF12, leaves the N-terminus of LCOR free for ligand responsive interaction with nuclear hormone receptors.

ASXL1 and ASXL2 define optional PR-DUB complexes containing OGT1 and FOXK transcription factors

The Drosophila PcG complex PR-DUB was identified as a heterodimer consisting of the deubiquitinase Calypso and the Asx protein[15]. However, the composition of its human counterpart remains elusive. Thus, we set out to systematically characterize this complex by performing purifications of BAP1, ASXL1 and ASXL2, the human homologs of the Drosophila PR-DUB components. Our AP-MS analysis revealed that BAP1 reciprocally interacts with both ASXL1 and ASXL2 (Fig. 3b). Interestingly, the two ASXL proteins do not interact with each other (Fig. 3b), suggesting the existence of two mutually exclusive PR-DUB complexes, which we called PR-DUB.1 and PR-DUB.2 depending on the ASXL partner of BAP1 being ASXL1 and ASXL2, respectively.

Both PR-DUB core components share a similar set of accessory proteins encompassing the transcription factors FOXK1 and FOXK2, the chromatin associated proteins MBD5 and MBD6, the transcriptional co-regulator HCFC1 and most notably OGT1 (Fig. 3b). A recent attempt to identify BAP1 interaction partners led to the identification of Asxl1, Asxl2, Ogt, Foxk1, Kdm1b and Hcf1 in mouse spleen tissue[76]. Our data provide support to these results and indicate a general, cell type independent assembly of mammalian PR-DUB complexes. Furthermore, our data clearly implicate OGT1 as member of mammalian PR-DUB complexes, an interaction which was not identified in the Drosophila PR-DUB complex purification[15] although the Drosophila homolog Ogt was previously annotated as bona fide PcG protein[44].

OGT1 is the only O-linked N-acetylglucosamine (O-GlcNAc) transferase in mammals. The enzyme catalyzes the addition of a single GlcNAc molecule to serine and threonine of many target proteins[77]. OGT1 enzymatic activity is required for mouse development and is essential for embryonic stem cell (ESC) viability[78]. In addition, the protein was found to interact with BAP1 and to localize to chromatin via its interaction with the 5-methylcytosine oxidase TET1[76,78]. To further refine the connectivity of OGT1 within the PR-DUB network, we performed AP-MS experiments using OGT1 as bait.

This analysis validated the interaction between BAP1 and OGT1 and the interactions of OGT1 with TET1 and NCOAT (Fig. 3b), the O-GlcNAcase counteracting OGT1 activity[78,79]. Moreover, our data identified a second set of OGT1-containing complexes involved in transcriptional regulation that did not co-purify with PR-DUB core subunits (Fig. 3b). These include the ZNFs ZEP1 and ZEP2, and the arginine-specific HMT CARM1. Furthermore, we identified OGT1 as subunit of WDR5 containing complexes. Indeed, OGT1 exhibits interactions with the NSL complex and with the SET1 HMT family activating complex WDR5/RBBP5/ASH2L, which is likely to mediate the interaction of OGT1 with MLL1 and SET1A (Fig. 3b). Although no interaction of OGT1 with FOXK1/2 and MBD5/6 was detected, these proteins co-cluster with PR-DUB core components and OGT1 is highly connected to the PR-DUB core (Fig. 3a-b).

These results suggest that OGT1/HCFC1 and FOXK/MBD proteins may form optional PR-DUB.1/PR-DUB.2 complexes. Conversely, OGT1 interactions with FOXK and MBD proteins could be transient and hence difficult to pinpoint by OGT1 affinity purification.

Genomics profiling of the FOXK1-containing PR-DUB.1

A functional interaction of OGT1 with FOXK transcription factors within the same PR-DUB complex would require their colocalization at genomic target sites. To test

this hypothesis, we examined the genome-wide distribution of O-GlcNAc, a proxy for catalytically active OGT1, ASXL1 and FOXK1 by performing ChIP-seq in HEK293 cells (Supplementary Fig. 6a).

By pairwise analysis of overlapping peak regions we found 41% and 55% of FOXK1 peaks co-localizing with O-GlcNAc and ASXL1, respectively, while 69% of O-GlcNAc peaks were co-occupied by ASXL1 (Fig. 4a). In total, we identified 2703 genomic loci bound by all three features (Fig. 4a). Functional annotation of these sites to genomic compartments revealed a predominant binding of PR-DUB.1 to gene promoters (Fig. 4a), with read densities sharply peaking at TSSs of RefSeq annotated genes (Fig. 4b). Moreover, we found that feature enrichments within ±1kb of TSSs are highly correlated to each other (>0.8), further indicating that ASXL1, FOXK1 and OGT1 are likely subunits of the same protein complex (Fig. 4c). To identify classes of genes bound by PR-DUB.1, we subjected the set of TSSs bound by each complex member to MSigDB pathway enrichment analysis. This analysis identified highly overlapping sets of enriched pathways for each protein (Supplementary Fig. 6b). Notably, PR-DUB.1 targets are predominantly enriched for genes involved in fundamental cellular processes like gene expression, cell cycle, mitosis and protein metabolism (Fig. 4d).

PRC1 complexes and PR-DUB.1 regulate different target genes

Mutations in Drosophila sxc (the gene encoding Ogt), calypso and Asx genes lead to de-repression of HOX genes and previous studies reported a strong colocalization of PR-DUB and O-GlcNAc with major PRC1 bound sites at inactive genes in Drosophila[15,44]. We sought to investigate this relation in the human genome by comparing our PR-DUB profiles with publicly available ChIP-seq data of RING2 and RYBP[23], as well as TIF1B[80].

Our analysis therefore focused on six representatives of the three major modules within our PcG interaction network at the chromatin level: RING2 and RYBP, the central core of the PRC1 module (Fig. 1c); TIF1B, the common component of ZNFs containing CBX1/3/5 complexes (Supplementary Fig. 4a), and PR-DUB.1. Besides the expected high correlation between RING2 and RYBP (p=0.78, Supplementary Fig. 6c), analysis of pairwise correlations of feature enrichments at promoters revealed a clear segregation between PRC1 and TIF1B on the one hand, and PR-DUB.1 on the other hand (Fig. 4e-f and Supplementary Fig. 6c). Similarly, when comparing the genome-wide distribution of PR-DUB.1 (2703 ASXL1+GlcNAc+FOXK1 co-occupied regions) with ?PRC1? (6816 RING2+RYBP peaks) and TIF1B (10297 peaks), we observed only a partial co-localization of these three complexes at target sites, with 24% and 31% of PR-DUB.1 binding sites co-bound by PRC1 and TIF1B, respectively and only 336 regions occupied by all three complexes (Fig. 4f).

In summary, our analysis uncovered the basic topology of the human PR-DUB network at both proteomics and genomics level. Interestingly, and in contrast to Drosophila, the human PR-DUB and PRC1 complexes bind largely distinct sets of target genes, strongly suggesting they are involved in different cellular processes in mammals. In addition, our AP-MS experiments identified the transcription factors FOXK1 and FOXK2 as components of PR-DUB, hence highlighting a potential recruitment mechanism of PR-DUB complexes. We anticipate that future experiments based on our data will shed light on the functionality of PR-DUB complexes in gene regulation and their relation to PRC1 and PRC2.

Conclusions

Although considerable progress has been made in determining the composition of mammalian PcG protein complexes, recent findings are primarily based on studies of isolated

protein components in different cellular contexts with heterogenous biochemical workflows, thus hampering a system-level understanding of gene silencing. In this study, in contrast, we used a systematic proteomic approach to comprehensively map the PcG protein interactome in a single human cell line. Since the abundance of PcG proteins can vary between cell types and surely influences the assembly of alternative protein complexes, we chose HEK293 cells for our study as all PcG proteins are expressed in this cell type. The result is a high-density interaction network, which enabled us to dissect individual PcG complexes with unprecedented detail. By allocating newly identified interaction partners to all PcG complex families and by identifying candidate subunits responsible for complex targeting to chromatin, we obtained new insights into molecular function and recruitment of the PcG silencing system. In addition to the fine mapping of the cardinal PcG complexes PRC1 and PRC2, our data unravel human PR-DUB as multifaceted assembly comprising OGT1 along with several transcription and chromatin binding factors. For the first time, our study testifies the significant diversity that exists among individual PcG complexes in a single cell line. In addition, it provides a solid framework for future systematic experiments aiming at disentangling the biochemistry of PcG protein-mediated gene regulation in mammalian cells.

Methods

Expression constructs and generation of stable cell lines

To generate expression vectors for tetracycline-induced expression of N-terminally SH-tagged bait proteins, human ORFs within pDONR223 vectors were picked from a Gateway-compatible human orfeome collection (horfeome v5.1, Open Biosystems) for LR recombination with the customized destination vector pcDNA5/FRT/TO/SH/GW, which was obtained through ligation of the SH-tag coding sequence and the Gateway recombination cassette into the polylinker of pcDNA5/FTR/TO (Invitrogen). Genes not in the human orfeome collection were amplified from human cDNA prepared from HEK293 cells by PCR and cloned into entry vectors by TOPO (pENTR/D-TOPO) reaction. Stable Flp-In HEK293 T-REx cell lines were generated as described in Supplementary Methods.

Protein purification

Stable Flp-In HEK293 T-REx cell lines were grown in five 14.5 cm Greiner dishes to 80% confluency and bait protein expression induced by the addition of 1μg/ml of tetracycline to the medium 16-24hrs prior to harvest in PBS containing 1 mM EDTA. The suspended cells were pelleted and drained from the supernatant for subsequent shock-freezing in liquid nitrogen and long term storage at -80°C. The frozen cell pellets were resupended in 5ml TNN lysis buffer (100 mM Tris pH 8.0, 5 mM ETDA, 250 mM NaCl, 50 mM NaF, 1% Igepal CA-630 (Nonidet P-40 Substitute), 1.5 mM Na3VO4, 1 mM PMSF, 1mM DTT and 1x Protease Inhibitor mix (Roche)) and rested on ice for 10 min. Insolubilizable material was removed by centrifugation. Cleared lysates were loaded on a pre-equilibrated spin column (Biorad) containing 200 μl Strep-Tactin sepharose (IBA Biotagnology). The sepharose was washed four times with 1 ml TNN lysis buffer (Igepal CA-630 and DTT concentrations adjusted to 0.5% and 0.5mM, respectively). Bound proteins were eluted with 1 ml 2 mM Biotin in TNN lysis buffer (Igepal CA-630 and DTT concentrations adjusted to 0.5% and 0.5mM, respectively), incubated for 2h with 100 μl HA-Agarose (Sigma), washed four times with TNN lysis buffer (Igepal CA-630 concentration adjusted to 0.5%, w/o DTT and w/o protease inhibitors) and two additional times in TNN buffer (100 mM Tris pH 8.0, 150 mM NaCl, 50 mM NaF).

The bound proteins were released by acidic elution with 500 μl 0.2 M Glycine pH 2.5 and the eluate was pH neutralized with NH4HCO3. Cysteine bonds were reduced with 5 mM TCEP for 30 min at 37°C and alkylated in 10 mM iodacetamide for 20 min at room temperature in the dark. Samples were digested with 1 μg trypsin (Promega) overnight at 37°C. Bait proteins with low protein yield were processed by single step purification, omitting the HA step. The frozen cell pellets were resuspended in 5ml of TNN lysis buffer containing 10 μg/ml Avidin. The eluates were TCA precipitated to remove biotin and resolubilized in 50 μl 10% ACN, 50 mM NH4HCO3 pH 8.8. After dilution with NH4HCO3 to 5% ACN the samples were reduced, alkylated and digested as in the double step protocol. The digested peptides were puri?ed with C18 microspin columns (The Nest Group Inc.) according to the protocol of the manufacturer, resolved in 0.1% formic acid, 1% acetonitrile for mass spectrometry analysis.

Mass spectrometry

LC-MS/MS analysis was performed on an LTQ Orbitrap XL mass spectrometer (Thermo Fisher Scientific). Peptide separation was carried out by reverse phase a Proxeon EASY-nLC II liquid chromatography system (Thermo Fisher Scientific). The reverse phase column (75 μm x 10 cm) was packed with Magic C18 AQ (3 μm) resin (WICOM International). A linear gradient from 5% to 35% mobile phase (98% acetonitrile, 0.1% formic acid) was run for 60 min over a stationary phase (0.1% formic acid, 2% acetonitrile) at a ?ow rate of 300 nl/min. Data acquisition was set to obtain one high resolution MS scan in the Orbitrap (60,000 @ 400 m/z) followed by six collision-induced fragmentation (CID) MS/MS fragment ion spectra in the linear trap quadrupole (LTQ). Orbitrap charge state screening was enabled and ions with unassigned or single charge states were rejected. The dynamic exclusion window was set to 15s and limited to 300 entries. The minimal precursor ion count to trigger CID and MS/MS scan was set to 150. The ion accumulation time was set to 500 ms (MS) and 250 ms (MS/MS) using a target setting of 106 (MS) and 104 (MS/MS) ions. After every biological replicate measurement, a peptide reference sample containing 200 fmol of human [Glu1]-Fibrinopeptide B (Sigma-Aldrich) was analyzed to monitor the overall LC-MS/MS systems performance.

ChIP and preparation of ChIP-seq libraries

Chromatin fixation and immunoprecipitation were performed essentially as described[81]. Cells (3-4x10^8) were fixed in 200 ml of medium with 1% formaldehyde for 10 min at room temperature. Cross-linked cells were sonicated to produce chromatin fragments of an average size of 150-400 bp. Soluble chromatin was separated from insoluble material by centrifugation. The supernatant containing chromatin of 1-2x10^7 cells was used for immunoprecipitation. Sequencing libraries were prepared with the NEB Genomic DNA Sample Preparation Kit according to NEB?s instructions. After adapter ligation, library fragments of 250-350 bp were isolated from an agarose gel. The DNA was PCR amplified with Illumina primers with 18 cycles, purified, and loaded on an Illumina flow cell for cluster generation. Libraries were sequenced on the Genome Analyzer IIx (TrueSeq cBot-GA v2 and TruSeq v5 SBS kit) and HiSeq 2000 (HiSeq Flow Cell v3 and TruSeq SBS Kit v3) following the manufacturer?s protocols. For ChIP-qPCR, nuclei were prepared essentially as described in *Functional Analysis of DNA and Chromatin*[82]. Immunoprecipitations were performed using Anti-GAL4 (sc-510, Santa Cruz Biotechnology), Anti-IgG (10500C, Invitrogen) and Anti-H3K27me3 kindly provided by Thomas Jenuwein. Anti-FOXK1 (ab18196) was purchased from Abcam , Anti-ASXL1 (sc85283) from Santa Cruz Biotechnology and Anti-GlcNAc (HGAC85) from Novus Biologicals. Primer sets used for qPCR are listed in the Supplemental Experimental Procedures.

Data analysis

Description of data processing and analysis methods are available in the Supplementary Methods.

Accession Numbers

Mass spectrometry data have been submitted to the PeptideAtlas database `http://www.peptideatlas.org/` and assigned the identifier PASS00347. Protein interactions have been submitted to the IMEx (`http://www.imexconsortium.org`) consortium through IntAct83 and assigned the identifier IM-21659. Sequencing data have been submitted to the NCBI Gene Expression Omnibus (`http://www.ncbi.nlm.nih.gov/geo`) under accession no. GSE51673.

Acknowledgements

We thank I. Nissen and M. Kohler for technical support on ChIP-seq. Illumina sequencing was done in the Genomics Facility Basel at D-BSSE, ETH Zürich. Research of SH and MG is supported by the European Union 7th Framework project SYBILLA (Systems Biology of T-cell activation) and the Innovative Medicines Initiative project ULTRA-DD. Research of RA is funded by advanced ERC grant Proteomics v3.0 (233226) and by SystemsX.ch, the Swiss initiative for systems biology. Research of RP is funded by the Swiss National Science Foundation and the ETH Zürich.

References

1. Sarkies, P. & Sale, J.E. Cellular &epigenetic stability and cancer. Trends in genetics 28, 118-127 (2012).
2. Ringrose, L. Polycomb comes of age: genome-wide profiling of target sites. Current opinion in cell biology 19, 290-297 (2007).
3. Jaenisch, R. & Young, R. Stem cells, the molecular circuitry of pluripotency and nuclear reprogramming. Cell 132, 567-582 (2008).
4. Maurange, C., Lee, N. & Paro, R. Signaling meets chromatin during tissue regeneration in Drosophila. Current opinion in genetics & development 16, 485-489 (2006).
5. Sparmann, A. & van Lohuizen, M. Polycomb silencers control cell fate, development and cancer. Nature reviews. Cancer 6, 846-856 (2006).
6. Cao, R. et al. Role of histone H3 lysine 27 methylation in Polycomb-group silencing. Science 298, 1039-1043 (2002).
7. Muller, J. et al. Histone methyltransferase activity of a Drosophila Polycomb group repressor complex. Cell 111, 197-208 (2002).
8. Fischle, W. et al. Molecular basis for the discrimination of repressive methyl-lysine marks in histone H3 by Polycomb and HP1 chromodomains. Genes & development 17, 1870-1881 (2003).
9. Min, J., Zhang, Y. & Xu, R.M. Structural basis for specific binding of Polycomb chromodomain to histone H3 methylated at Lys 27. Genes & development 17, 1823-1828 (2003).
10. de Napoles, M. et al. Polycomb group proteins Ring1A/B link ubiquitylation of histone H2A to heritable gene silencing and X inactivation. Developmental cell 7, 663-676 (2004).
11. Stock, J.K. et al. Ring1-mediated ubiquitination of H2A restrains poised RNA polymerase II at bivalent genes in mouse ES cells. Nature cell biology 9, 1428-1435 (2007).
12. Wang, H. et al. Role of histone H2A ubiquitination in Polycomb silencing. Nature 431, 873-878 (2004).
13. Klymenko, T. et al. A Polycomb group protein complex with sequence-specific DNA-binding

and selective methyl-lysine-binding activities. Genes & development 20, 1110-1122 (2006).
14. Lagarou, A. et al. dKDM2 couples histone H2A ubiquitylation to histone H3 demethylation during Polycomb group silencing. Genes & development 22, 2799-2810 (2008).
15. Scheuermann, J.C. et al. Histone H2A deubiquitinase activity of the Polycomb repressive complex PR-DUB. Nature 465, 243-247 (2010).
16. Furuyama, T., Banerjee, R., Breen, T.R. & Harte, P.J. SIR2 is required for polycomb silencing and is associated with an E(Z) histone methyltransferase complex. Current biology 14, 1812-1821 (2004).
17. Saurin, A.J., Shao, Z., Erdjument-Bromage, H., Tempst, P. & Kingston, R.E. A Drosophila Polycomb group complex includes Zeste and dTAFII proteins. Nature 412, 655-660 (2001).
18. Strubbe, G. et al. Polycomb purification by in vivo biotinylation tagging reveals cohesin and Trithorax group proteins as interaction partners. Proceedings of the National Academy of Sciences of the United States of America 108, 5572-5577 (2011).
19. Beisel, C. et al. Comparing active and repressed expression states of genes controlled by the Polycomb/Trithorax group proteins. Proceedings of the National Academy of Sciences of the United States of America 104, 16615-16620 (2007).
20. Enderle, D. et al. Polycomb preferentially targets stalled promoters of coding and noncoding transcripts. Genome research 21, 216-226 (2011).
21. Oktaba, K. et al. Dynamic regulation by polycomb group protein complexes controls pattern formation and the cell cycle in Drosophila. Developmental cell 15, 877-889 (2008).
22. Schuettengruber, B. et al. Functional anatomy of polycomb and trithorax chromatin landscapes in Drosophila embryos. PLoS biology 7, e13 (2009).
23. Gao, Z. et al. PCGF homologs, CBX proteins, and RYBP define functionally distinct PRC1 family complexes. Molecular cell 45, 344-356 (2012).
24. Margueron, R. et al. Ezh1 and Ezh2 maintain repressive chromatin through different mechanisms. Molecular cell 32, 503-518 (2008).
25. Shen, X. et al. EZH1 mediates methylation on histone H3 lysine 27 and complements EZH2 in maintaining stem cell identity and executing pluripotency. Molecular cell 32, 491-502 (2008).
26. Vandamme, J., Volkel, P., Rosnoblet, C., Le Faou, P. & Angrand, P.O. Interaction proteomics analysis of polycomb proteins defines distinct PRC1 complexes in mammalian cells. Molecular & cellular proteomics 10, M110 002642 (2011).
27. Sanchez, C. et al. Proteomics analysis of Ring1B/Rnf2 interactors identifies a novel complex with the Fbxl10/Jhdm1B histone demethylase and the Bcl6 interacting corepressor. Molecular & cellular proteomics 6, 820-834 (2007).
28. Bernstein, E. et al. Mouse polycomb proteins bind differentially to methylated histone H3 and RNA and are enriched in facultative heterochromatin. Molecular and cellular biology 26, 2560-2569 (2006).
29. Farcas, A.M. et al. KDM2B links the Polycomb Repressive Complex 1 (PRC1) to recognition of CpG islands. eLife 1, e00205 (2012).
30. He, J. et al. Kdm2b maintains murine embryonic stem cell status by recruiting PRC1 complex to CpG islands of developmental genes. Nature cell biology 15, 373-384 (2013).
31. Wu, X., Johansen, J.V. & Helin, K. Fbxl10/Kdm2b recruits polycomb repressive complex 1 to CpG islands and regulates H2A ubiquitylation. Molecular cell 49, 1134-1146 (2013).
32. Morey, L., Aloia, L., Cozzuto, L., Benitah, S.A. & Di Croce, L. RYBP and Cbx7 define specific biological functions of polycomb complexes in mouse embryonic stem cells. Cell reports 3, 60-69 (2013).
33. Morey, L. et al. Nonoverlapping functions of the Polycomb group Cbx family of proteins in embryonic stem cells. Cell stem cell 10, 47-62 (2012).
34. Tavares, L. et al. RYBP-PRC1 complexes mediate H2A ubiquitylation at polycomb target sites independently of PRC2 and H3K27me3. Cell 148, 664-678 (2012).
35. Hunkapiller, J. et al. Polycomb-like 3 promotes polycomb repressive complex 2 binding to CpG islands and embryonic stem cell self-renewal. PLoS genetics 8, e1002576 (2012).

36. Sarma, K., Margueron, R., Ivanov, A., Pirrotta, V. & Reinberg, D. Ezh2 requires PHF1 to efficiently catalyze H3 lysine 27 trimethylation in vivo. Molecular and cellular biology 28, 2718-2731 (2008).
37. Kim, H., Kang, K. & Kim, J. AEBP2 as a potential targeting protein for Polycomb Repression Complex PRC2. Nucleic acids research 37, 2940-2950 (2009).
38. Kim, T.G., Kraus, J.C., Chen, J. & Lee, Y. JUMONJI, a critical factor for cardiac development, functions as a transcriptional repressor. The Journal of biological chemistry 278, 42247-42255 (2003).
39. Pasini, D. et al. JARID2 regulates binding of the Polycomb repressive complex 2 to target genes in ES cells. Nature 464, 306-310 (2010).
40. Peng, J.C. et al. Jarid2/Jumonji coordinates control of PRC2 enzymatic activity and target gene occupancy in pluripotent cells. Cell 139, 1290-1302 (2009).
41. Shen, X. et al. Jumonji modulates polycomb activity and self-renewal versus differentiation of stem cells. Cell 139, 1303-1314 (2009).
42. Glatter, T., Wepf, A., Aebersold, R. & Gstaiger, M. An integrated workflow for charting the human interaction proteome: insights into the PP2A system. Molecular systems biology 5, 237 (2009).
43. Varjosalo, M. et al. Interlaboratory reproducibility of large-scale human protein-complex analysis by standardized AP-MS. Nature methods 10, 307-314 (2013).
44. Gambetta, M.C., Oktaba, K. & Muller, J. Essential role of the glycosyltransferase sxc/Ogt in polycomb repression. Science 325, 93-96 (2009).
45. Craig, R. & Beavis, R.C. TANDEM: matching proteins with tandem mass spectra. Bioinformatics 20, 1466-1467 (2004).
46. Deutsch, E.W. et al. A guided tour of the Trans-Proteomic Pipeline. Proteomics 10, 1150-1159 (2010).
47. Behrends, C., Sowa, M.E., Gygi, S.P. & Harper, J.W. Network organization of the human autophagy system. Nature 466, 68-76 (2010).
48. Cai, Y. et al. Subunit composition and substrate specificity of a MOF-containing histone acetyltransferase distinct from the male-specific lethal (MSL) complex. The Journal of biological chemistry 285, 4268-4272 (2010).
49. Migliori, V., Mapelli, M. & Guccione, E. On WD40 proteins: propelling our knowledge of transcriptional control? Epigenetics 7, 815-822 (2012).
50. Gao, Z. et al. An AUTS2-Polycomb complex activates gene expression in the CNS. Nature 516, 349-354 (2014).
51. van den Boom, V. et al. Non-canonical PRC1.1 Targets Active Genes Independent of H3K27me3 and Is Essential for Leukemogenesis. Cell reports 14, 332-346 (2016).
52. van den Boom, V. et al. Nonredundant and locus-specific gene repression functions of PRC1 paralog family members in human hematopoietic stem/progenitor cells. Blood 121, 2452-2461 (2013).
53. Miyata, Y. & Nishida, E. DYRK1A binds to an evolutionarily conserved WD40-repeat protein WDR68 and induces its nuclear translocation. Biochimica et biophysica acta 1813, 1728-1739 (2011).
54. Morita, K., Lo Celso, C., Spencer-Dene, B., Zouboulis, C.C. & Watt, F.M. HAN11 binds mDia1 and controls GLI1 transcriptional activity. Journal of dermatological science 44, 11-20 (2006).
55. Dietrich, N. et al. REST-mediated recruitment of polycomb repressor complexes in mammalian cells. PLoS genetics 8, e1002494 (2012).
56. El Messaoudi-Aubert, S. et al. Role for the MOV10 RNA helicase in polycomb-mediated repression of the INK4a tumor suppressor. Nature structural & molecular biology 17, 862-868 (2010).
57. Ogawa, H., Ishiguro, K., Gaubatz, S., Livingston, D.M. & Nakatani, Y. A complex with chromatin modifiers that occupies E2F- and Myc-responsive genes in G0 cells. Science 296,

1132-1136 (2002).
58. Qin, J. et al. The polycomb group protein L3mbtl2 assembles an atypical PRC1-family complex that is essential in pluripotent stem cells and early development. Cell stem cell 11, 319-332 (2012).
59. Trojer, P. et al. L3MBTL2 protein acts in concert with PcG protein-mediated monoubiquitination of H2A to establish a repressive chromatin structure. Molecular cell 42, 438-450 (2011).
60. Dou, Y. et al. Regulation of MLL1 H3K4 methyltransferase activity by its core components. Nature structural & molecular biology 13, 713-719 (2006).
61. Wysocka, J. et al. A PHD finger of NURF couples histone H3 lysine 4 trimethylation with chromatin remodelling. Nature 442, 86-90 (2006).
62. Zhang, P., Lee, H., Brunzelle, J.S. & Couture, J.F. The plasticity of WDR5 peptide-binding cleft enables the binding of the SET1 family of histone methyltransferases. Nucleic acids research 40, 4237-4246 (2012).
63. Junco, S.E. et al. Structure of the polycomb group protein PCGF1 in complex with BCOR reveals basis for binding selectivity of PCGF homologs. Structure 21, 665-671 (2013).
64. Sanchez-Pulido, L., Devos, D., Sung, Z.R. & Calonje, M. RAWUL: a new ubiquitin-like domain in PRC1 ring finger proteins that unveils putative plant and worm PRC1 orthologs. BMC genomics 9, 308 (2008).
65. Beisel, C. & Paro, R. Silencing chromatin: comparing modes and mechanisms. Nature reviews. Genetics 12, 123-135 (2011).
66. Alekseyenko, A.A., Gorchakov, A.A., Kharchenko, P.V. & Kuroda, M.I. Reciprocal interactions of human C10orf12 and C17orf96 with PRC2 revealed by BioTAP-XL cross-linking and affinity purification. Proceedings of the National Academy of Sciences of the United States of America 111, 2488-2493 (2014).
67. Kalb, R. et al. Histone H2A monoubiquitination promotes histone H3 methylation in Polycomb repression. Nature structural & molecular biology 21, 569-571 (2014).
68. Margueron, R. & Reinberg, D. The Polycomb complex PRC2 and its mark in life. Nature 469, 343-349 (2011).
69. Caubit, X. et al. Mouse Dac, a novel nuclear factor with homology to Drosophila dachshund shows a dynamic expression in the neural crest, the eye, the neocortex, and the limb bud. Developmental dynamics 214, 66-80 (1999).
70. Wu, K. et al. Cell fate determination factor DACH1 inhibits c-Jun-induced contact-independent growth. Molecular biology of the cell 18, 755-767 (2007).
71. Fernandes, I. et al. Ligand-dependent nuclear receptor corepressor LCoR functions by histone deacetylase-dependent and -independent mechanisms. Molecular cell 11, 139-150 (2003).
72. Shi, Y. et al. Coordinated histone modifications mediated by a CtBP co-repressor complex. Nature 422, 735-738 (2003).
73. Hansen, K.H. et al. A model for transmission of the H3K27me3 epigenetic mark. Nature cell biology 10, 1291-1300 (2008).
74. Cai, L. et al. An H3K36 methylation-engaging Tudor motif of polycomb-like proteins mediates PRC2 complex targeting. Molecular cell 49, 571-582 (2013).
75. Musselman, C.A. et al. Molecular basis for H3K36me3 recognition by the Tudor domain of PHF1. Nature structural & molecular biology 19, 1266-1272 (2012).
76. Dey, A. et al. Loss of the tumor suppressor BAP1 causes myeloid transformation. Science 337, 1541-1546 (2012).
77. Hart, G.W., Slawson, C., Ramirez-Correa, G. & Lagerlof, O. Cross talk between O-GlcNAcylation and phosphorylation: roles in signaling, transcription, and chronic disease. Annual review of biochemistry 80, 825-858 (2011).
78. Vella, P. et al. Tet proteins connect the O-linked N-acetylglucosamine transferase Ogt to chromatin in embryonic stem cells. Molecular cell 49, 645-656 (2013).
79. Whisenhunt, T.R. et al. Disrupting the enzyme complex regulating O-GlcNAcylation blocks signaling and development. Glycobiology 16, 551-563 (2006).

80. Iyengar, S., Ivanov, A.V., Jin, V.X., Rauscher, F.J., 3rd & Farnham, P.J. Functional analysis of KAP1 genomic recruitment. Molecular and cellular biology 31, 1833-1847 (2011).
81. Orlando, V., Strutt, H. & Paro, R. Analysis of chromatin structure by in vivo formaldehyde cross-linking. Methods 11, 205-214 (1997).
82. Santoro, R. Analysis of chromatin composition of repetitive sequences: the ChIP-Chop assay. Methods Mol Biol 1094, 319-328 (2014).
83. Orchard, S. et al. The MIntAct project–IntAct as a common curation platform for 11 molecular interaction databases. Nucleic acids research 42, D358-363 (2014).
84. McLean, C.Y. et al. GREAT improves functional interpretation of cis-regulatory regions. Nature biotechnology 28, 495-501 (2010).

Figure Legends

Figure 1. Systematic profiling of human Polycomb group (PcG) protein complexes. (a) Workflow for native protein complex purifications from Flp-In HEK293 T-REx cells. Open reading frames of 64 bait proteins were cloned into an expression vector containing a tetracycline inducible CMV promoter, Strep-HA fusion tag, and FRT sites. Proteins were affinity purified from whole cell extracts of isogenic cell lines, trypsinized and identified by tandem mass spectrometry on an LTQ Orbitrap XL. High confidence interaction proteins (HCIPs) were hierarchically clustered to infer protein complex compositions. (b) Hierarchical clustering of HCIPs. Clusters of PcG and non-PcG complexes are labeled in red and blue, respectively. The inset shows the location of PRC1.1, PRC1.3/PRC1.5 and the four core proteins RYBP/YAF2 and RING1/2. Clusters defined by single baits are indicated in green. Spearman's rank correlation coefficient based dissimilarities are color coded as indicated (top right). (c) Protein-protein interaction network of clustered interaction data. Blue lines indicate interactions between proteins within the same cluster. Enlarged hexagon-shaped nodes correspond to the baits used in this study. (d-e) High-density interaction maps of PRC1.3/PRC1.5 (d) and PRC1.6 (e). New subunits are highlighted by dashed boxes. Hexagon shaped nodes represent baits; squares: identified HCIPs not used as baits in this study. Black nodes: common core subunits; yellow nodes: DNA binding proteins.

Figure 2. High-resolution interaction analysis unravels two structurally distinct classes of PRC2 complexes. (a) Excerpt of Figure 1b showing the PRC2 cluster. (b) Interaction map of PRC2 components. The PRC2 core is highlighted by a dashed box. Reciprocal interactions defining the two classes of PRC2 complexes are indicated in blue (PRC2.1) and red (PRC2.2) edges. Orange edges: non-reciprocal interactions. (c) Schematic representation of alternative protein isoforms of LCOR and C10ORF12. Numbers indicate amino acid positions. (d) LCOR interaction map. Orange edges, interactions defined in this study; dashed edges, published interactions. (e) Schematic representation of the employed luciferase reporter system. Amplicons (TSS, +500) used for ChIP-qPCR analysis are indicated. (f) Anti-Gal4 Western Blot showing the expression of Gal4-C10ORF12 and Gal4-LCOR upon tetracycline induction (g) Luciferase activity of tetracycline-induced Gal4-C10ORF12 and Gal4-LCOR expressing cells, normalized to uninduced cells. Values are mean?sd, p-values are from a two-sided t-test (n=7). (h) Anti-Gal4 ChIP-qPCR analysis showing localization of C10ORF12 and LCOR to the reporter TSS. (i) Anti-H3K27me3 ChIP-qPCR analysis at the reporter TSS upon C10ORF12 and LCOR expression. Values are mean±sd, p-values are from a two-sided t-test (n=3).

Figure 3. Human PR-DUB complexes contain OGT1 and FOXK transcription factors. (a) Excerpt of Figure 1b showing the PR-DUB and 19S proteasome

clusters. (b) Topology of PR-DUB complexes. Interactions of bait proteins with proteins localized in PR-DUB cluster are indicated in blue. WDR5 shares many interacting proteins with OGT1 (indicated in red), which are predominantly MLL/SET complex associated proteins, and does not interact with BAP1, ASXL1 and 2. Hexagons: bait proteins; squares, identified HCIPs not used as baits in this study. Yellow: FOXK1 and 2. Orange nodes: OGT1 interactors. Dashed line: ASXL2-MBD5 interaction, which was detected but did not pass our stringent filtering criteria.

Figure 4. PR-DUB.1 and PRC1 target largely distinct set of genes. (a) Venn diagrams showing the genome-wide colocalization of high-confidence peaks for the PR-DUB.1 components FOXK1 (blue), ASXL1 (orange) and the O-GlcNAc modification (green). Empirical p-values from peak shuffling are indicated, along with the percentage of intersecting peaks for each feature. The pie chart illustrates the distribution of PR-DUB.1 peaks (2703, triple intersection) with respect to TSSs. (b) Average ChIP-seq signal (normalized to total library size) of FOXK1, ASXL1, O-GlcNAc within a 5 kb window centered on RefSeq TSS. (c) Pairwise correlation of PR-DUB.1 feature enrichments at TSSs. Spearman's rank correlation coefficients are indicated. (d) Functional annotation of high-confidence PR-DUB.1 peaks localizing within 5 kb of annotated TSSs. Top 10 significantly enriched MSigDB pathways obtained with GREAT84 are indicated. UCSC tracks of PR-DUB.1 ChIP-seq signals at representative promoters belonging to the top three hits are shown in order of significance (encoded by blue tones). (e) Heatmap of ChIP-seq signals (normalized to total library size) for the indicated features within 10 kb of PR C1 and PR-DUB.1 binding sites. (f) Venn diagrams showing the genome-wide colocalization of high-confidence PR-DUB.1 peaks (red), PRC1 (brown) and TIF1B (light blue). A representative UCSC track of ChIP-Seq signals at TSSs bound by all three features is shown.

Supplementary Figure Legends

Supplementary Figure 1. Comparison of AP-MS interaction data with public protein interaction databases and high resolution interaction map of SKP1 and WDR5. (a) Compilation of human bait proteins used for AP-MS and their relation to core subunits of Drosophila PcG complexes. (b) Number of high confidence interacting proteins (HCIPs) for each bait. Dark blue bars represent interactions annotated in the public protein interaction database IntAct, light blue bars are novel interactions found in this study (overall 75%). (c) SKP1 interactome inferred in this study (blue and orange lines) and annotated in public literature databases (red dotted lines). The thick blue lines represent the main interactions to PcG components that cluster together with SKP1 and form PRC1.1. About half of the identified interactions (n = 42) were F-box proteins, including KDM2B - the only F-box protein associated with the PRC1.1 complex. Hexagons indicate bait, squares prey proteins. (d) WDR associated proteins overlapping with[1]. Uniprot protein names and number of proteins are indicated. (e) Interaction map of WDR5 AP-MS results. Blue lines represent interactions detected in this study to PcG associated proteins that cluster with WDR5 and form PRC1.6. Interactions with other HCIPs (orange) together with public literature interactions (dotted red lines) could be assigned to known protein complexes (MLL, TCP, NSL, TORC2 and ADA2/GCN5/ADA3 transcription activator complex). Hexagons indicate bait, squares prey proteins.

Supplementary Figure 2. High-resolution topology maps of selected clusters. (a) RBBP4/7 interaction proteome. In addition to interacting with PRC2 and HP1, RBBP4/7 proteins were found to bind members of the LINC, NURF, NURD and SIN3 complexes. (b) No human Pho-RC could be identified. TYY1 and SMBT1, the homologs of the Drosphila Pho-RC proteins Pho and dSFMBT, respectively, did not interact. However, TYY1 co-purified with the INO80 complex, which is indicated by a dashed circle. (c) Interaction proteome of the four human LMBL paralogs. Only LMBL2 exhibited interactions with a PcG protein assembly and is part of PRC1.6. In all panels blue and orange lines represent interactions found in this study; red dashed lines are annotated public literature interactions. Hexagons indicate bait, squares prey proteins.

Supplementary Figure 3. Network topology of PRC1 complexes. (a) Protein-protein interactions among the central core proteins of the PRC1 complexes. Note that we detected no interactions between protein paralogs. Edges represent detected reciprocal interactions. (b) Network topology of PRC1.2 and PRC1.4 complexes. Note that PCGF2/4 can assemble to PRC1.2/PRC1.4 or can form trimeric complexes (edges in red) with RING1/2 and RYBP/YAF2 (we detect no interactions between RYBP/YAF2 with CBX and PHC proteins). Edges connecting PRC1.2/PRC1.4 core components in blue. (c) Excerpt of Figure 2A indicating the allocation of the WD40 protein DCAF7 to PRC1.3/PRC1.5. High-density interaction maps of PRC1.3/PRC1.5 (C) and PRC1.6 (D). New subunits are highlighted by dashed boxes. Hexagon shaped nodes represent baits; squares: identified HCIPs not used as baits in this study. Black nodes: common core subunits; yellow nodes: DNA binding proteins. (d) PRC1.1 complex contains PCGF1 and SKP1 and links the co-repressors BCOR and BCORL as well as the demethylase KDM2B to the PRC1.1 core. Edges connecting core components are in purple.

Supplementary Figure 4. Interaction proteomes of PRC1 and HP1 complexes. (a) CBX1/3/5 interactions with zinc finger (ZNF; orange nodes) and neighboring proteins. Note that all bait proteins of this subnetwork interacted with the nuclear co-repressor TIF1B (yellow), which underscores the reported function of TIF1B in the

recruitment of HP1 proteins to specific DNA sequences through interaction with zinc finger transcription factors. Hexagons indicate bait, squares prey proteins. Blue edges, interactions of potential core subunits of the corresponding network, interactions in public databases as dashed lines, others in orange. (b) CBX1 and CBX3 but not CBX5 interact with the histone methyltransferases EHMT1 and EHMT2. The CBX1/3-EHMT1/2 complex also interacts with zinc finger transcription factors WIZ, ZN644, ZN462 and the co-repressor protein TIF1B. In contrast to a previous report we did not detect any potential interactions of EHMT1/2 with PRC1.6[2]. (c) Interaction of CBX3 and CBX5 with SENP7. This complex may also include TIF1B, the zinc finger transcription factor AHDC1 and the histone chaperone CHAP1. (d) CBX1/3/5 complex with histone chaperone CAF1 and RBBP4, which is potentially involved in DNA replication. (e) Centromeric DSN1/MIS12 complex with HP1 proteins, involved in mitosis.

Supplementary Figure 5. Characterization of PRC2 core interacting proteins C17ORF96 and C10ORF12. (a) C17ORF96 and SKDA1 are related proteins, which share sequence similarity at their C-terminus. BLAST search result with C17ORF96 (Uniprot A6NHQ4) as query sequence. (b) CLUSTAL 2.1 alignment of C17ORF96 (Uniprot A6NHQ4) and SKDA1 (Uniprot Q1XH10) amino acid sequences. Homologous C-termini, identified by BLAST search, indicated in red. (c) All AP-MS identified peptides that match to LCOR-CRA_b. Colors indicate specific protein regions as in Fig. 2c. (d) Number of identified LCOR and C10ORF12 isoform peptides in PRC2 protein purification experiments. (e) Number of PRC2 prey peptides in LCOR and C10ORF12 isoform AP-MS experiments. (f) C10ORF12 localize in the nucleus. Images show anti-HA in situ stainings of stable Flp-In HEK293 T-REx cell lines before and after tetracycline induction. HA-EGFP shows a dispersed, cytoplasmic signal whereas the C10ORF12 HA-epitope fusion protein shows a nuclear signal. In situ stainings were performed as described in Glatter et al., 2009[3].

Supplementary Figure 6. Functional annotation of PR-DUB.1 components binding sites and genome-wide analysis of PR-DUB.1, PRC1 and TIF1B enrichments at TSSs. (a) Sequence read statistics of ChIP-seq experiments. (b) Functional annotation of high-confidence MACS peaks localizing within 5kb of annotated TSSs. Enriched MSigDB pathways were computed with GREAT[4]. (c) Pairwise scatter plots of PR-DUB.1, PRC1 and TIF1B enrichments at TSSs. Spearman's rank correlation coefficients are indicated.

Supplementary Methods

Cell Line Generation

Flp-In HEK293 T-REx cells (Invitrogen) containing a single genomic FRT site and stably expressing the tet repressor were cultured in DMEM (4.5 g/l glucose, 10% FCS, 2 mM L-glutamine) containing 100 μg/ml zeocin and 15 μg/ml blasticidin. The medium was exchanged with DMEM medium containing 15 μg/ml blasticidin before transfection. For cell line generation, Flp-In HEK293 T-REx cells were co-transfected with the corresponding expression plasmids and the pOG44 vector (Invitrogen) for co-expression of the Flp-recombinase using the Lipofectamine 2000 transfection reagent (Invitrogen). Two days after transfection, cells were selected in hygromycin-containing medium (100 μg/ml) for 2-3 weeks.

Protein Identification

Mass spectrometry raw data were searched with X!Tandem[5] against a human protein sequence database (Swiss-Prot canonical reviewed human proteome reference data set; `http://www.uniprot.org/`), including reverse decoy sequences for all entries. The search parameters were set to include only fully tryptic peptides (KR/P) containing up to two missed cleavages. Peptide modifications consisted of Carbamidomethyl (+57.021465 amu) on Cys (static) and oxidation (+15.99492 amu) on Met (dynamic) and phosphorylation (+79.966331 amu) on Ser, Thr, Tyr (dynamic) were set as dynamic peptide modifications. Precursor mass error tolerance was set to 25 ppm, the fragment mass error tolerance to 0.5 Da. Obtained peptide spectrum matches were statistically evaluated using PeptideProphet and protein inference by ProteinProphet, both part of the Trans Proteomic Pipeline[6]. A minimum protein probability of 0.9 was set to match a false discovery rate (FDR) of <1%. The resulting pep.xml and prot.xml files were used as input for the spectral counting software tool Abacus7 to calculate spectral counts and normalized spectral abundance factor (NSAF) values[8,9].

Evaluation of high confidence interacting proteins (HCIP)

Adjusted NSAF values of identified co-purified proteins were compared to a control data set of 62 StrepHA-GFP and 12 StrepHA-RFP-NLS purification experiments. The protein abundance in the control data set was estimated by averaging the 10 highest NSAF values per protein among all 74 measurements. Protein abundance enrichment of >10 fold compared to the control data set was used as an initial step for filtering protein interaction raw data. Adjusted NSAF values were also used to calculate WDN-scores of all the interaction candidates[10]. A simulated data matrix was used to calculate the WD-score threshold below which 98% of the simulated data falls. From this high confidence interaction data set (control ratio > 10; WDN-score > 1) a distance matrix was calculated with the Multiple Experiment Viewer[11] (`http://www.tm4.org/mev/`) using an uncentered Pearson distance metric and mapped on the unfiltered raw interactions. To relax filtering stringency in close proximity in the network, sub-threshold interactions (control ratio and WDN-score) were rescued if the distance was greater than zero (n = 314 protein interactions). The resulting filtered data set contained the high confidence interacting proteins (HCIPs) and corresponding protein-protein interactions. For comparison to literature data, all human protein interactions were extracted from the public database IntAct[12].

Clustering analysis

All data analyses were performed using R[13] (`http://www.R-project.org`). Agglomerative hierarchical clustering of HCIP was performed using adjusted NSAF values. Different correlation-based dissimilarity measures were considered in combination with commonly adopted intergroup dissimilarity measures (single, average and complete linkage functions). For each pair of measures, clustering performances were evaluated using the cophenetic correlation coefficient, which measures the ability of a dendrogram to represent the input data structure[14]. As a result of this procedure, hierarchical clustering was performed by adopting a Spearman's rank correlation coefficient based dissimilarity along with average linkage. Therefore, the dissimilarity between prey i and j was computed as $d_{ij} = (1 - r(x_i, x_j))/2$, where r is the SCC.

Network Visualization

Protein Interaction data were visualized with Cytoscape 2.8.3[15]. Known bait interactions were obtained from the protein interaction network analysis platform PINA v2 (December 2012)[16] using bait protein identifiers as starting nodes.

ChIP-Seq data analysis

ChIP-Seq profiles of RING1B, RYBP, TIF1B (GEO accession number GSM855007, GSM855008 and GSE27929, respectively) and corresponding input data sets were downloaded in sra format and converted to fastq using the NCBI Short Read Archive Toolkit. Short reads were aligned to the human genome (hg19 assembly) using Bowtie 2.0.0[17] allowing for 1 mismatch in a 30nt seed, reporting best out of at most 100 alignments. Overall alignment rates ranged between 83 and 94% for in-house generated data sets and between 75 and 98% for the others. Alignments were converted from SAM format to BAM using SAMtools 0.1.18[18]. Peak calling was performed using MACS 1.4.0[19] with default parameters. Peaks were then filtered according to p-values ($p < 10^{-10}$). If replicates were available, only peak intersections were considered further and denoted as high-confidence peaks. All subsequent analyses were performed using R/Bioconductor[20]. Coverage tracks at single base pair resolution were generated with wavClusteR[21]. Overlapping peaks were determined using GenomicRanges using a minimum overlap of 1bp. RefSeq transcript annotations were fetched from UCSC using GenomicFeatures. Unique TSSs were defined as TSSs having no other annotated TSS within their 1kb flanking region, irrespective of the strand. A total of 21612 unique TSSs was considered further. Metaprofiles of ChIP-Seq signals at TSSs ($\pm$ 2.5kb) were computed using non-overlapping windows of width 50 nt. ChIP-Seq signal heatmaps were computed with Genomation[22]. Feature enrichments at unique promoters were computed as described in[23]. MSigDB pathway analysis was performed with GREAT 2.0.2[4] by associating genomic regions to single nearest annotated genes within 5kb.

Supplementary References

1. Cai, Y. et al. Subunit composition and substrate specificity of a MOF-containing histone acetyltransferase distinct from the male-specific lethal (MSL) complex. The Journal of biological chemistry 285, 4268-4272 (2010).

2. Ogawa, H., Ishiguro, K., Gaubatz, S., Livingston, D.M. & Nakatani, Y. A complex with chromatin modifiers that occupies E2F- and Myc-responsive genes in G0 cells. Science 296, 1132-1136 (2002).

3. Glatter, T., Wepf, A., Aebersold, R. & Gstaiger, M. An integrated workflow for charting the human interaction proteome: insights into the PP2A system. Molecular systems biology 5, 237 (2009).

4. McLean, C.Y. et al. GREAT improves functional interpretation of cis-regulatory regions. Nature biotechnology 28, 495-501 (2010).

5. Craig, R. & Beavis, R.C. TANDEM: matching proteins with tandem mass spectra. Bioinformatics 20, 1466-1467 (2004).

6. Deutsch, E.W. et al. A guided tour of the Trans-Proteomic Pipeline. Proteomics 10, 1150-1159 (2010).

7. Fermin, D., Basrur, V., Yocum, A.K. & Nesvizhskii, A.I. Abacus: a computational tool for extracting and pre-processing spectral count data for label-free quantitative proteomic analysis. Proteomics 11, 1340-1345 (2011).

8. Paoletti, A.C. et al. Quantitative proteomic analysis of distinct mammalian Mediator complexes using normalized spectral abundance factors. Proceedings of the National Academy

of Sciences of the United States of America 103, 18928-18933 (2006).
9. Zybailov, B. et al. Statistical analysis of membrane proteome expression changes in Saccharomyces cerevisiae. Journal of proteome research 5, 2339-2347 (2006).
10. Behrends, C., Sowa, M.E., Gygi, S.P. & Harper, J.W. Network organization of the human autophagy system. Nature 466, 68-76 (2010).
11. Saeed, A.I. et al. TM4: a free, open-source system for microarray data management and analysis. BioTechniques 34, 374-378 (2003).
12. Orchard, S. et al. The MIntAct project–IntAct as a common curation platform for 11 molecular interaction databases. Nucleic Acids Research 42, D358-63 (2014).
13. R Core Team. R: A Language and Environment for Statistical Computing. Vienna, Austria. (2012).
14. Hastie, T., Tibshirani, R. & Friedman, J. The elements of statistical learning data mining, inference, and prediction, Edn. 2nd. (Springer, New York, N.Y.; 2009).
15. Shannon, P. et al. Cytoscape: a software environment for integrated models of biomolecular interaction networks. Genome research 13, 2498-2504 (2003).
16. Wu, J. et al. Integrated network analysis platform for protein-protein interactions. Nature methods 6, 75-77 (2009).
17. Langmead, B. & Salzberg, S.L. Fast gapped-read alignment with Bowtie 2. Nature methods 9, 357-359 (2012).
18. Li, H. et al. The Sequence Alignment/Map format and SAMtools. Bioinformatics 25, 2078-2079 (2009).
19. Zhang, Y. et al. Model-based analysis of ChIP-Seq (MACS). Genome biology 9, R137 (2008).
20. Huber, W. et al. Orchestrating high-throughput genomic analysis with Bioconductor. Nature methods 12, 115-121 (2015).
21. Comoglio, F., Sievers, C. & Paro, R. Sensitive and highly resolved identification of RNA-protein interaction sites in PAR-CLIP data. BMC bioinformatics 16, 32 (2015).
22. Akalin, A. et al. Genomation: a toolkit to summarize, annotate and visualize genomic intervals. Bioinformatics 31, 1127-1129 (2014).
23. Enderle, D. et al. Polycomb preferentially targets stalled promoters of coding and noncoding transcripts. Genome research 21, 216-226 (2011).

Figure 1

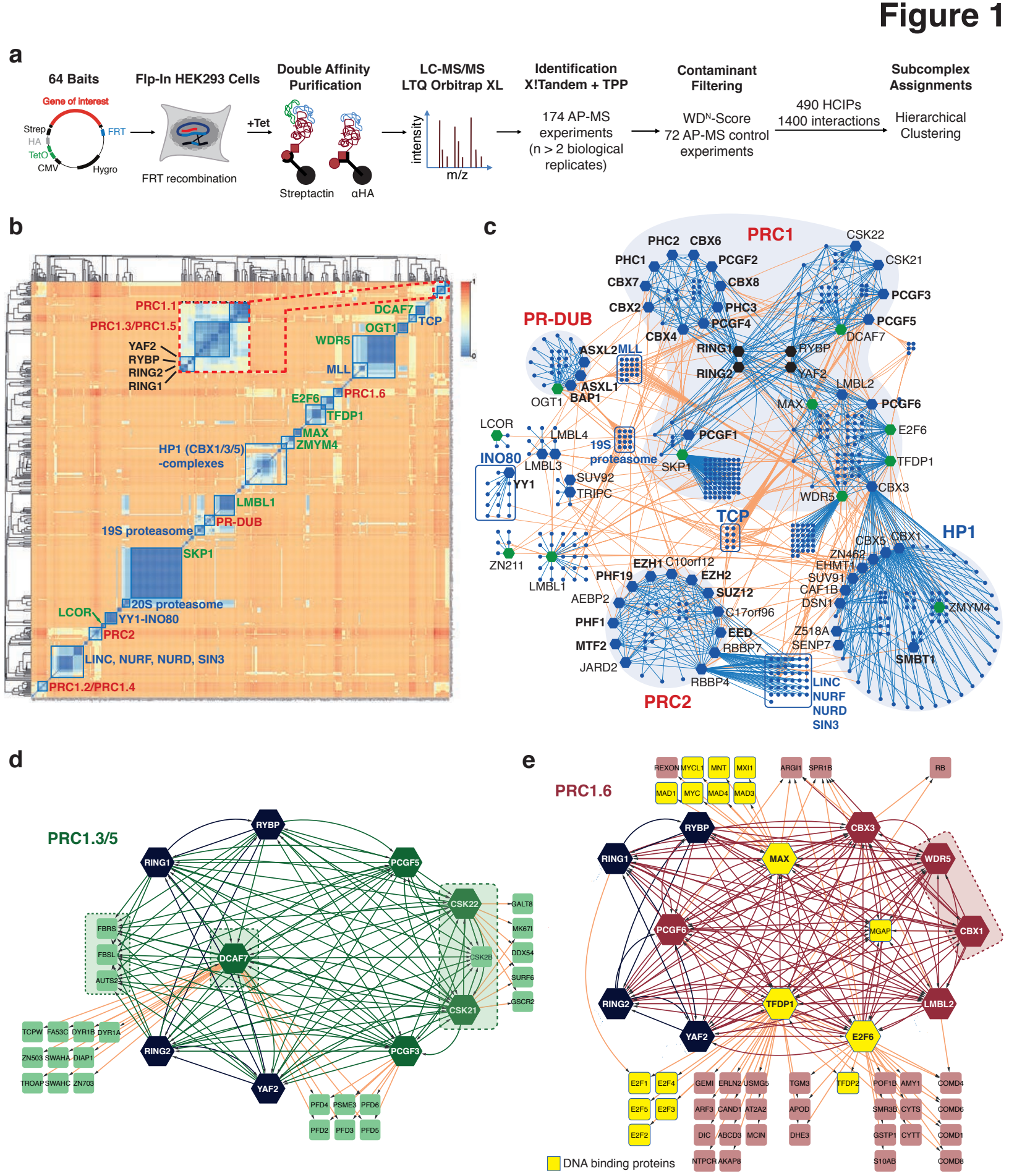
a
64 Baits
Flp-In HEK293 Cells
Double Affinity Purification
LC-MS/MS LTQ Orbitrap XL
Identification X!Tandem + TPP
Contaminant Filtering
Subcomplex Assignments
Gene of interest
Strep
HA
TetO
CMV
FRT
Hygro
FRT recombination
+Tet
Streptactin
αHA
intensity
m/z
174 AP-MS experiments (n > 2 biological replicates)
WD^N-Score
72 AP-MS control experiments
490 HCIPs
1400 interactions
Hierarchical Clustering
b
PRC1.1
PRC1.3/PRC1.5
YAF2
RYBP
RING2
RING1
DCAF7
TCP
OGT1
WDR5
MLL
PRC1.6
E2F6
TFDP1
MAX
ZMYM4
HP1 (CBX1/3/5) -complexes
LMBL1
PR-DUB
19S proteasome
SKP1
20S proteasome
LCOR
YY1-INO80
PRC2
LINC, NURF, NURD, SIN3
PRC1.2/PRC1.4
c
PRC1
PHC2
CBX6
PHC1
PCGF2
CBX7
CBX8
CBX2
PHC3
PCGF4
CBX4
RING1
RING2
RYBP
YAF2
CSK22
CSK21
PCGF3
PCGF5
DCAF7
PR-DUB
ASXL2
MLL
ASXL1
BAP1
OGT1
LMBL2
MAX
PCGF6
E2F6
TFDP1
CBX3
WDR5
LCOR
LMBL4
19S proteasome
PCGF1
SKP1
INO80
LMBL3
YY1
SUV92
TRIPC
TCP
HP1
CBX5
CBX1
ZN462
EHMT1
SUV91
CAF1B
DSN1
ZMYM4
Z518A
SENP7
SMBT1
ZN211
LMBL1
EZH1
C10orf12
EZH2
PHF19
AEBP2
SUZ12
C17orf96
PHF1
EED
MTF2
RBBP7
JARD2
RBBP4
PRC2
LINC
NURF
NURD
SIN3
d
PRC1.3/5
RYBP
RING1
PCGF5
CSK22
GALT8
MK67I
DDX54
SURF6
GSCR2
FBRS
FBSL
AUTS2
DCAF7
CSK2B
CSK21
TCPW
FA53C
DYR1B
DYR1A
ZN503
SWAHA
DIAP1
TROAP
SWAHC
ZN703
RING2
PCGF3
YAF2
PFD4
PSME3
PFD6
PFD2
PFD3
PFD5
e
PRC1.6
REXON
MYCL1
MNT
MXI1
ARGI1
SPR1B
RB
MAD1
MYC
MAD4
MAD3
RYBP
CBX3
RING1
MAX
WDR5
PCGF6
MGAP
CBX1
RING2
TFDP1
LMBL2
YAF2
E2F6
E2F1
E2F4
GEMI
ERLN2
USMG5
TGM3
TFDP2
POF1B
AMY1
COMD4
E2F5
E2F3
ARF3
CAND1
AT2A2
APOD
SMR3B
CYTS
COMD6
E2F2
DIC
ABCD3
MCIN
DHE3
GSTP1
CYTT
COMD1
NTPCR
AKAP8
S10AB
COMD8
DNA binding proteins

Figure 2

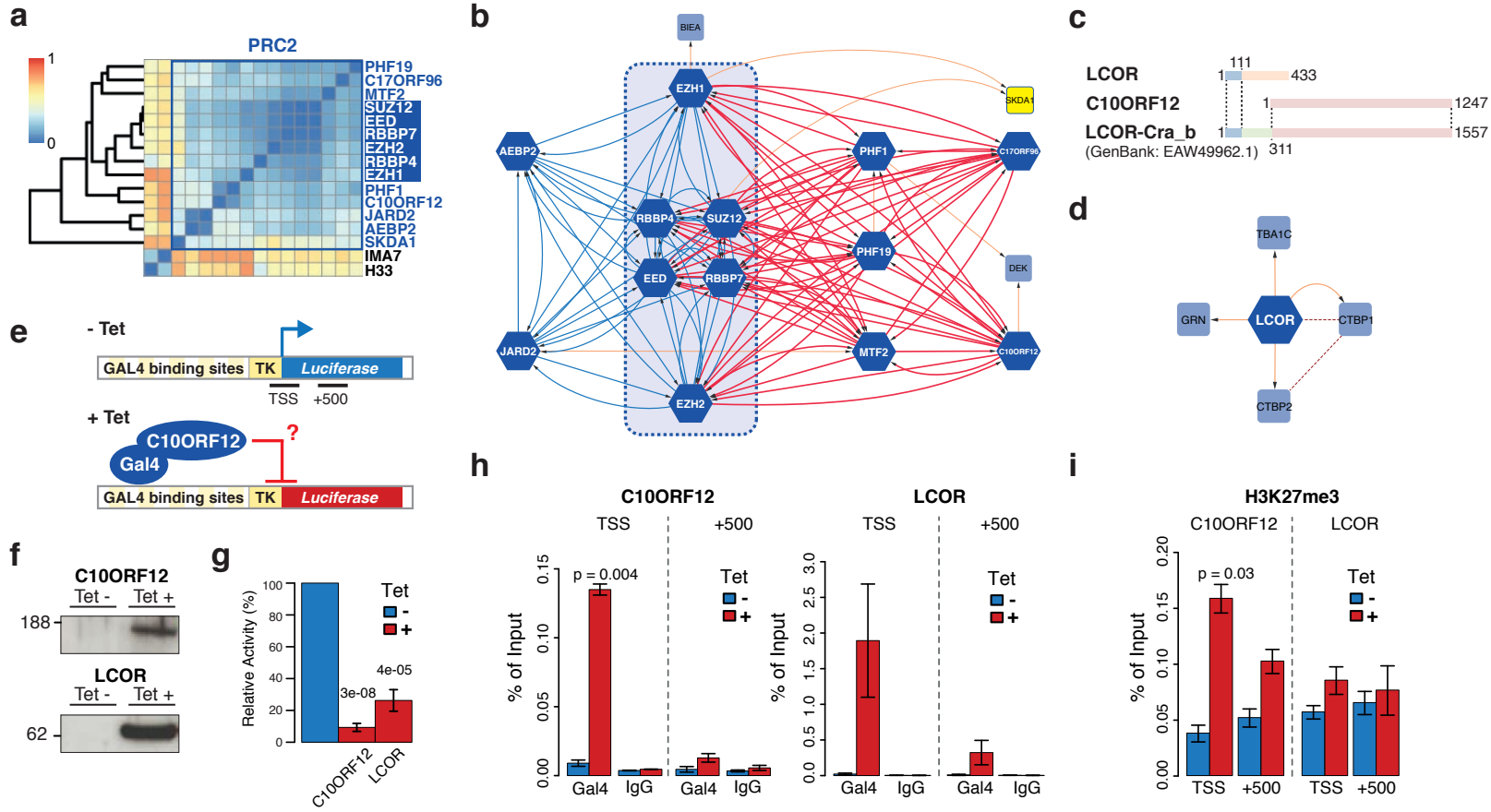
a
PRC2
1
0
PHF19
C17ORF96
MTF2
SUZ12
EED
RBBP7
EZH2
RBBP4
EZH1
PHF1
C10ORF12
JARD2
AEBP2
SKDA1
IMA7
H33
b
BIEA
EZH1
SKDA1
AEBP2
PHF1
C17ORF96
RBBP4
SUZ12
PHF19
EED
RBBP7
DEK
JARD2
MTF2
C10ORF12
EZH2
c
LCOR
1
111
433
C10ORF12
1
1247
LCOR-Cra_b
(GenBank: EAW49962.1)
1
311
1557
d
TBA1C
GRN
LCOR
CTBP1
CTBP2
e
- Tet
GAL4 binding sites
TK
Luciferase
TSS
+500
+ Tet
C10ORF12
Gal4
?
GAL4 binding sites
TK
Luciferase
f
C10ORF12
Tet -
Tet +
188
LCOR
Tet -
Tet +
62
g
Relative Activity (%)
100
80
60
40
20
0
Tet
-
+
3e-08
4e-05
C10ORF12
LCOR
h
C10ORF12
TSS
+500
LCOR
TSS
+500
% of Input
p = 0.004
Tet
-
+
Gal4
IgG
Gal4
IgG
Gal4
IgG
Gal4
IgG
i
H3K27me3
C10ORF12
LCOR
% of Input
p = 0.03
Tet
-
+
TSS
+500
TSS
+500

Figure 3

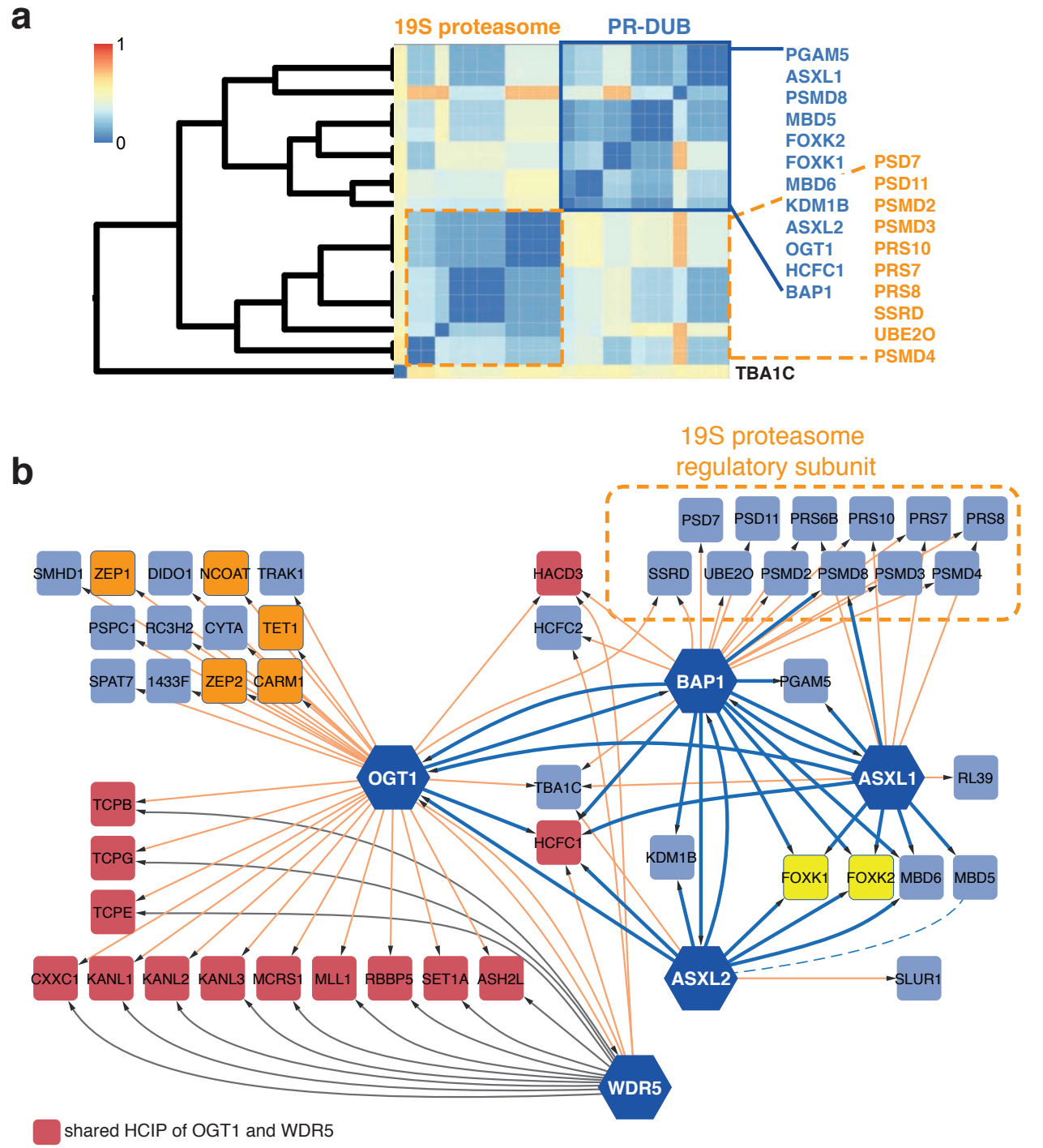
a
19S proteasome
PR-DUB
1
0
PGAM5
ASXL1
PSMD8
MBD5
FOXK2
FOXK1
MBD6
KDM1B
ASXL2
OGT1
HCFC1
BAP1
PSD7
PSD11
PSMD2
PSMD3
PRS10
PRS7
PRS8
SSRD
UBE2O
PSMD4
TBA1C
b
19S proteasome
regulatory subunit
PSD7
PSD11
PRS6B
PRS10
PRS7
PRS8
SSRD
UBE2O
PSMD2
PSMD8
PSMD3
PSMD4
SMHD1
ZEP1
DIDO1
NCOAT
TRAK1
PSPC1
RC3H2
CYTA
TET1
SPAT7
1433F
ZEP2
CARM1
HACD3
HCFC2
BAP1
PGAM5
OGT1
TBA1C
ASXL1
RL39
TCPB
TCPG
TCPE
HCFC1
KDM1B
FOXK1
FOXK2
MBD6
MBD5
CXXC1
KANL1
KANL2
KANL3
MCRS1
MLL1
RBBP5
SET1A
ASH2L
ASXL2
SLUR1
WDR5
shared HCIP of OGT1 and WDR5

Figure 4

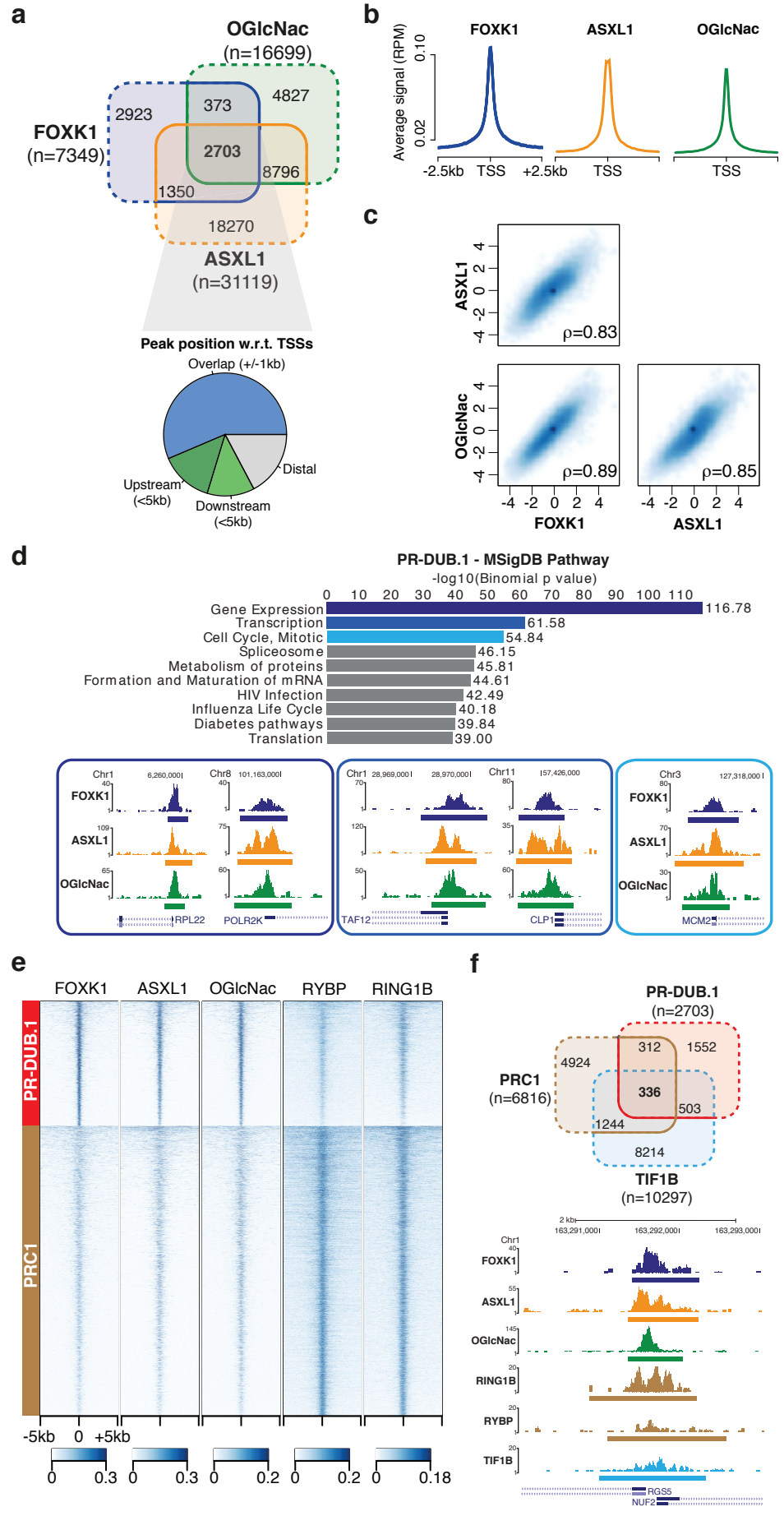
a
OGlcNac
(n=16699)
FOXK1
(n=7349)
ASXL1
(n=31119)
2923
373
4827
2703
8796
1350
18270
Peak position w.r.t. TSSs
Overlap (+/-1kb)
Distal
Upstream
(<5kb)
Downstream
(<5kb)
b
FOXK1
ASXL1
OGlcNac
Average signal (RPM)
0.10
0.02
-2.5kb
TSS
+2.5kb
TSS
TSS
c
ASXL1
OGlcNac
FOXK1
ASXL1
ρ=0.83
ρ=0.89
ρ=0.85
d
PR-DUB.1 - MSigDB Pathway
-log10(Binomial p value)
Gene Expression 116.78
Transcription 61.58
Cell Cycle, Mitotic 54.84
Spliceosome 46.15
Metabolism of proteins 45.81
Formation and Maturation of mRNA 44.61
HIV Infection 42.49
Influenza Life Cycle 40.18
Diabetes pathways 39.84
Translation 39.00
Chr1
Chr8
Chr11
Chr3
FOXK1
ASXL1
OGlcNac
RPL22
POLR2K
TAF12
CLP1
MCM2
e
FOXK1
ASXL1
OGlcNac
RYBP
RING1B
PR-DUB.1
PRC1
-5kb
0
+5kb
f
PR-DUB.1
(n=2703)
PRC1
(n=6816)
TIF1B
(n=10297)
4924
312
1552
336
503
1244
8214
FOXK1
ASXL1
OGlcNac
RING1B
RYBP
TIF1B
RGS5
NUF2

Supplementary Figure 1

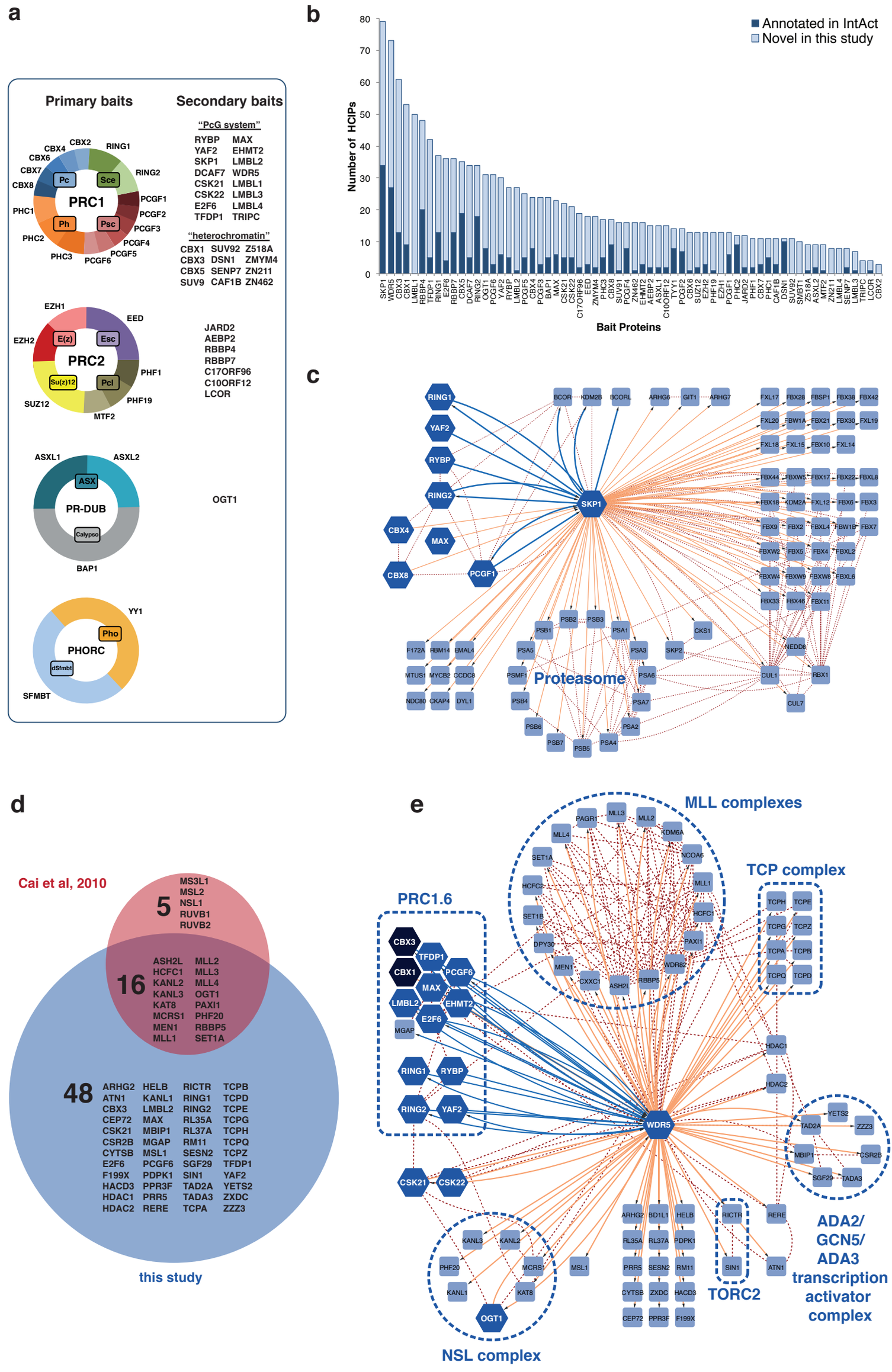

Supplementary Figure 2

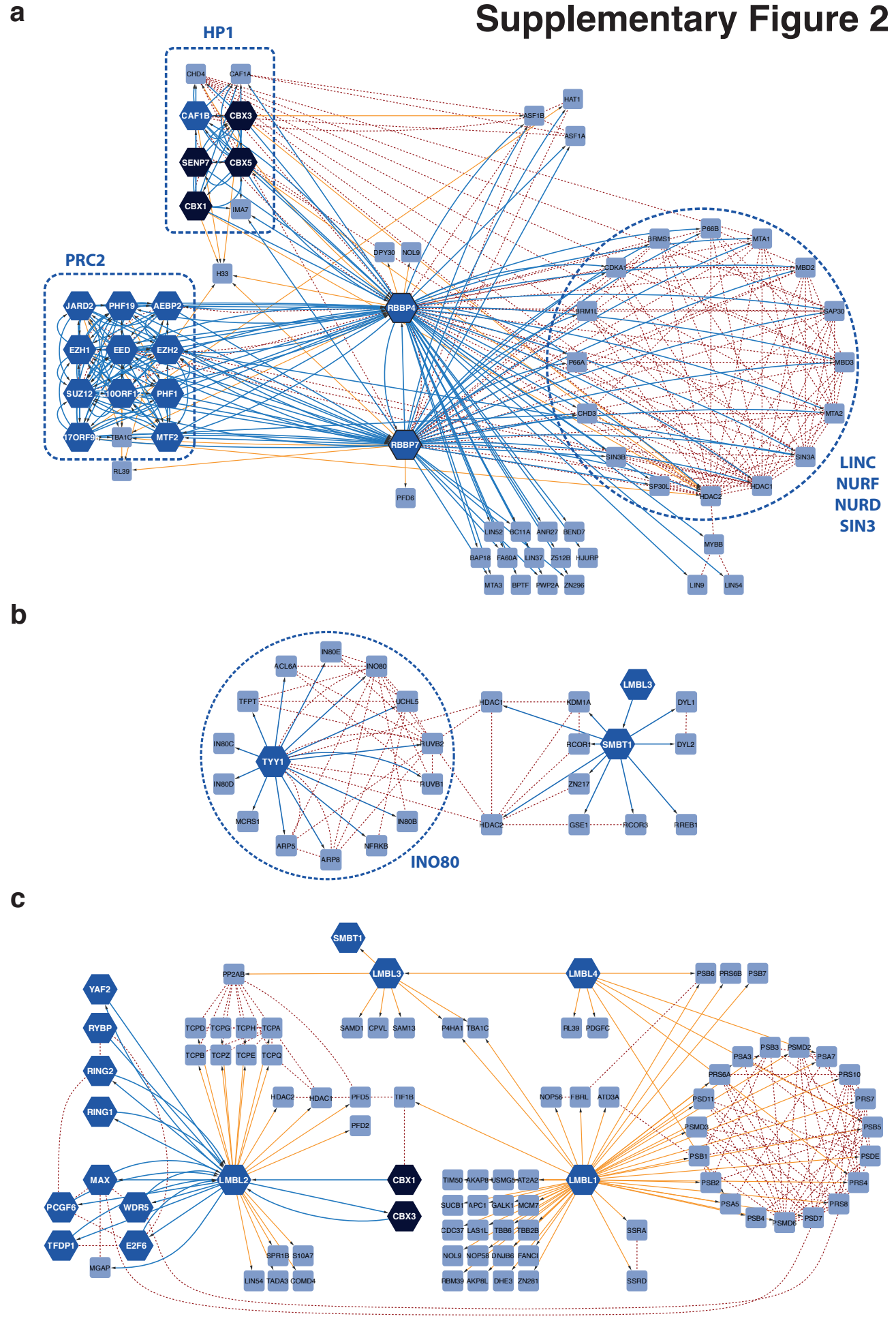

Supplementary Figure 3

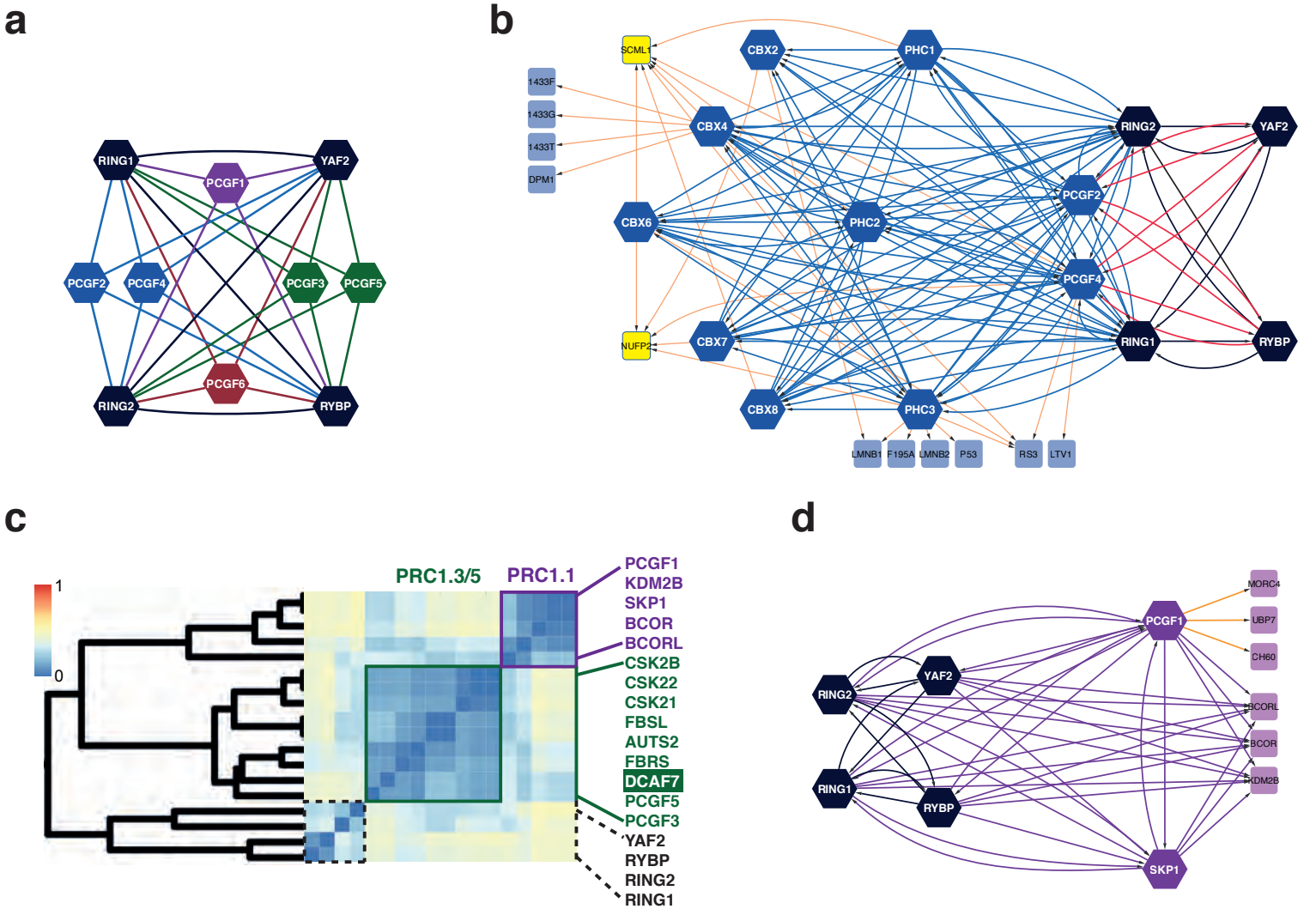

Supplementary Figure 4

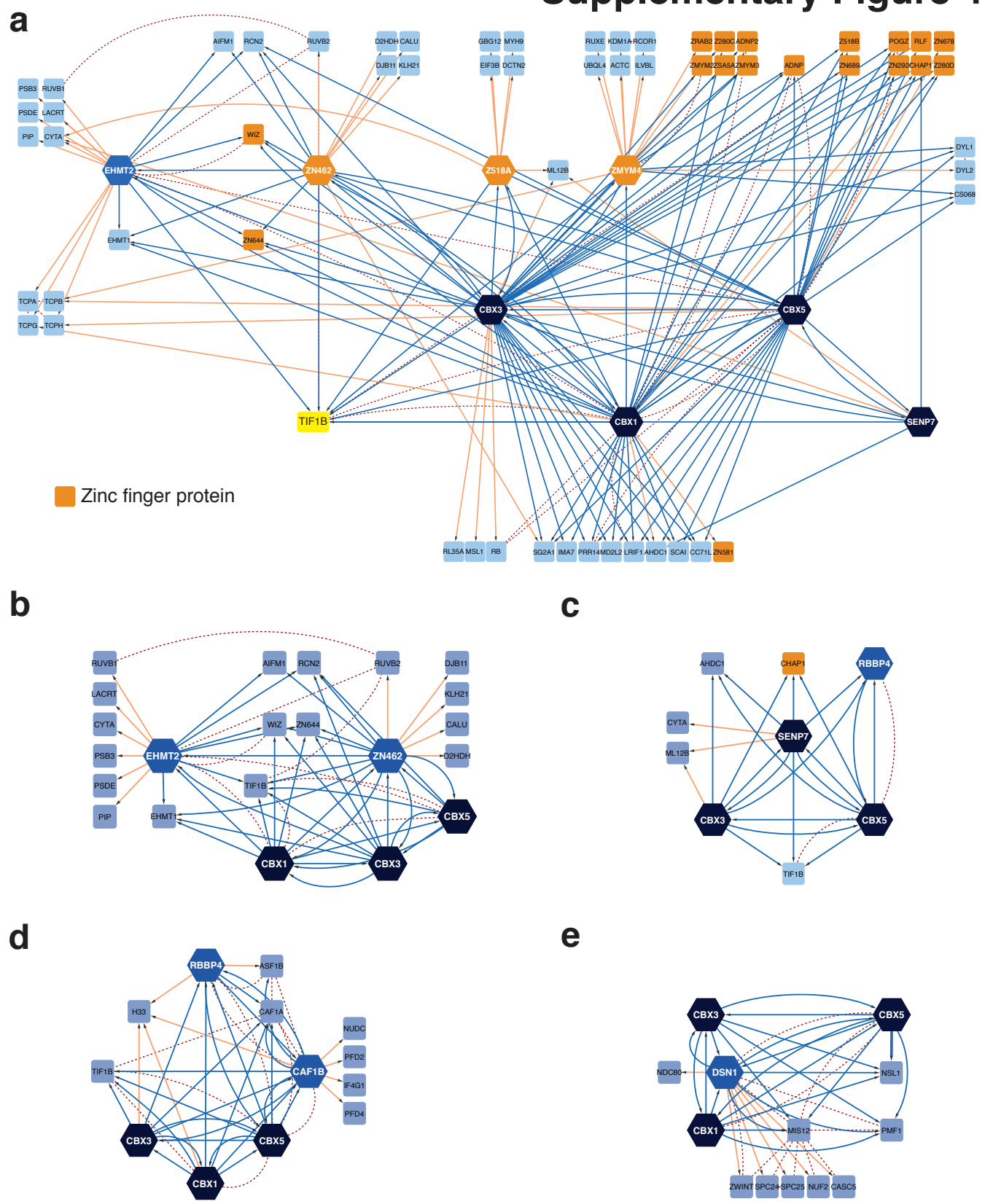

Supplementary Figure 5

a

Score	Expect	Method	Identities	Positives	Gaps
77.8 bits(190)	2e-14	Compositional matrix adjust.	34/64 (53%)	43/64 (67%)	1/64 (1%)

```
C17ORF96 313  FSLLNCFPCPPALVVGEDGDLKPASSLRLQGDSKPP-PAHPLWRWQMGGPAVPEPPGLKFWGIN  375
              F  +  FPCPP+L++G DGDL PA SL    DS+ P  AHP+W+WQ+GG A+P PP  KF   N
SKDA1    763  FHFMANFPCPPSLIIGRDGDLWPAYSLNTTKDSQTPHKAHPIWKWQLGGSAIPLPPSHKFRKFN  826
```

b

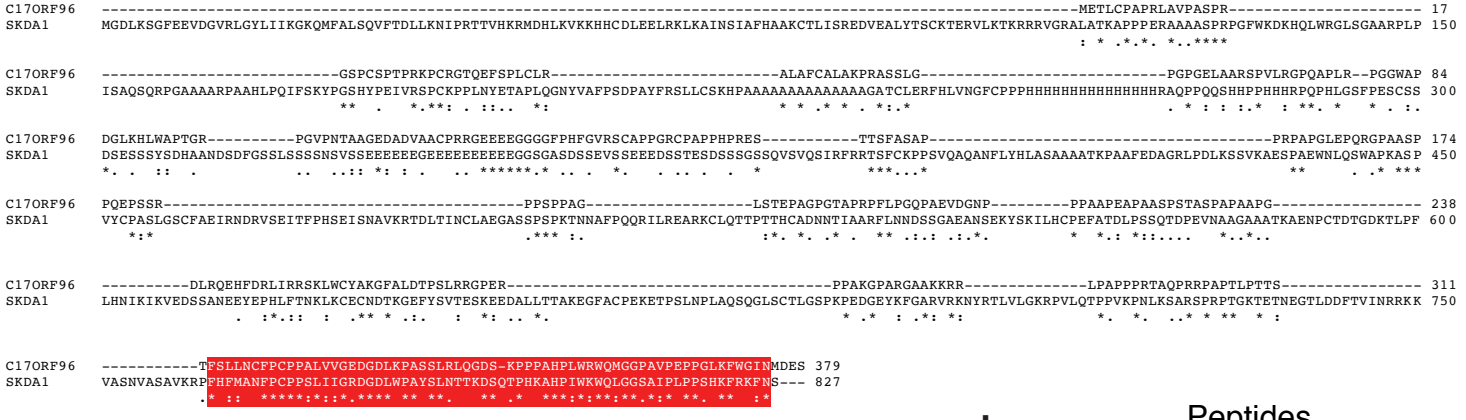

c

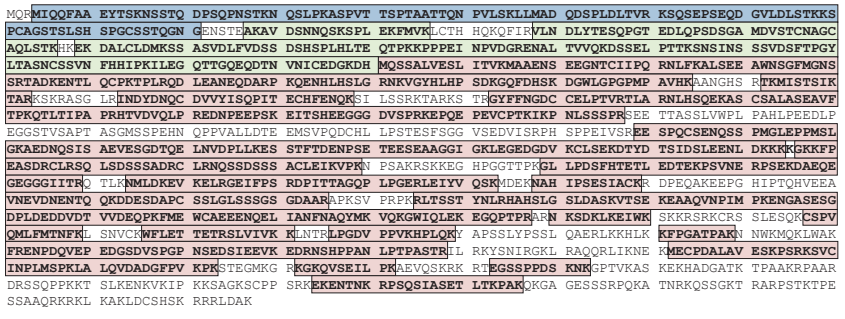

d

Peptides

Baits	LCOR-Cra/LCOR	LCOR-Cra	C10orf12	LCOR	Total
C10orf12	0	0	126	0	**126**
LCOR-Cra	18	14	85	0	**117**
EED	0	1	9	0	**10**
EZH1	1	2	16	0	**19**
EZH2	3	1	13	0	**17**
LCOR	40	0	0	95	**135**
MTF2	1	1	13	0	**15**
PHF1	3	1	28	0	**32**
PHF19	0	1	4	0	**5**
Total	**66**	**21**	**294**	**95**	**476**

e

Peptides

Baits	PRC2 interactions															LCOR interactions						
	C10orf12	LCOR-Cra	LCOR-Cra/LCOR	DEK	EED	EZH1	EZH1/EZH2	EZH2	MTF2	PHF1	PHF19	RBBP4	RBBP4/RBBP7	RBBP7	SUZ12	CTBP1	CTBP1/CTBP2	CTBP2	GRN	LCOR	TBA1C	Total
C10orf12	126	0	0	0	34	10	6	43	27	17	2	8	7	9	54	0	0	0	0	0	1	**344**
LCOR-Cra	85	14	18	2	19	0	3	19	17	10	0	4	5	3	23	0	0	0	0	0	2	**224**
LCOR	0	0	40	0	0	0	0	0	0	0	0	0	0	0	0	11	5	16	1	95	3	**171**
Total	**211**	**14**	**58**	**2**	**53**	**10**	**9**	**62**	**44**	**27**	**2**	**12**	**12**	**12**	**77**	**11**	**5**	**16**	**1**	**95**	**6**	**739**

f

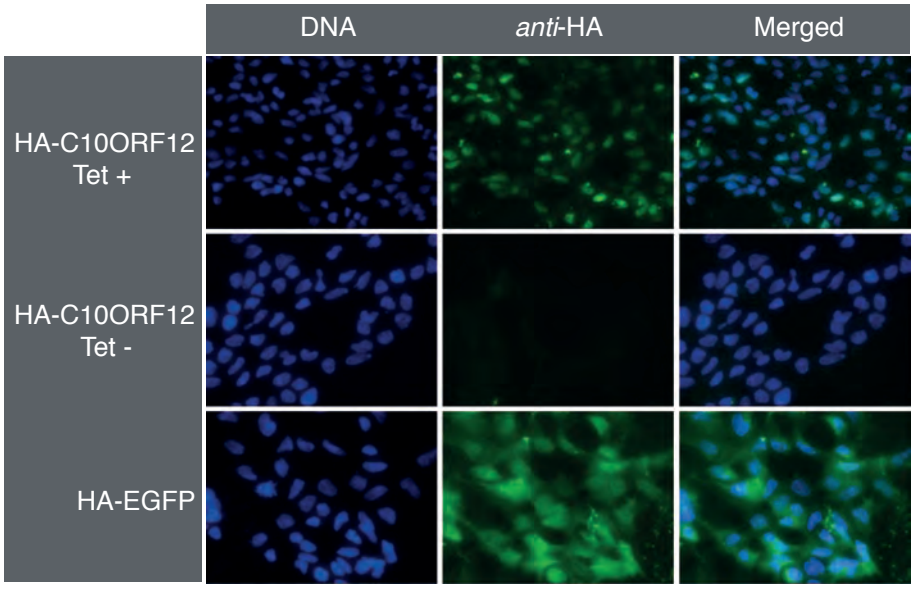

Supplementary Figure 6

a

Sample	Total reads (mio.)	Overall alignment (%)	Unique alignments (%)	Multiple alignments (%)
ASXL1	47.2	88.1	31.8 (67.4)	9.7 (20.7)
FOXK1	18.6	94.3	13.1 (70.3)	4.4 (24.0)
O-GlcNAc	46.2	86.4	30.2 (65.3)	9.8 (21.1)
Input62	20.2	97.4	13.4 (66.4)	6.3 (31.1)
Input63	46.8	83.8	27.7 (59.3)	11.5 (24.5)

b

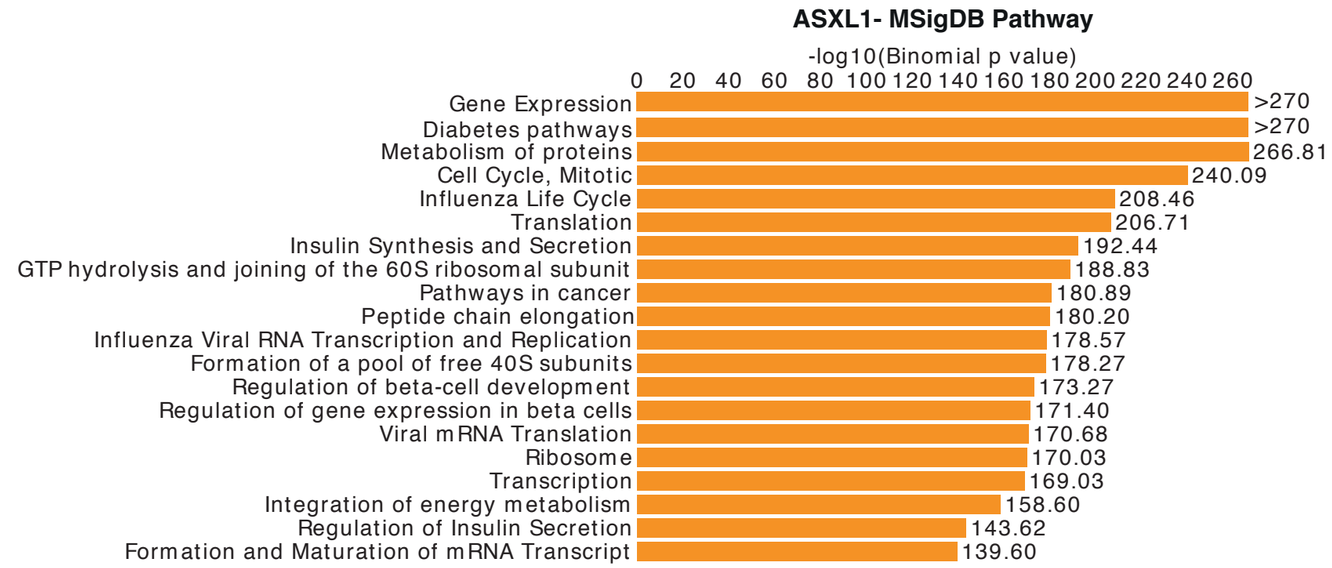
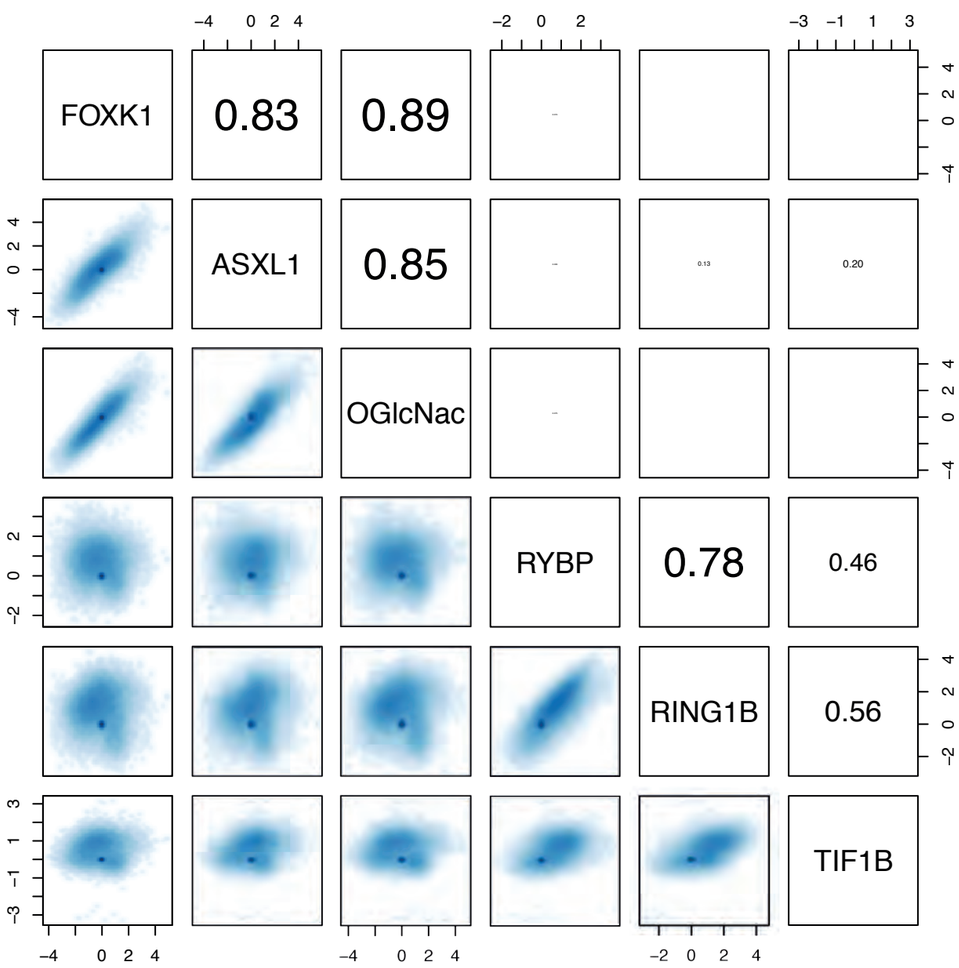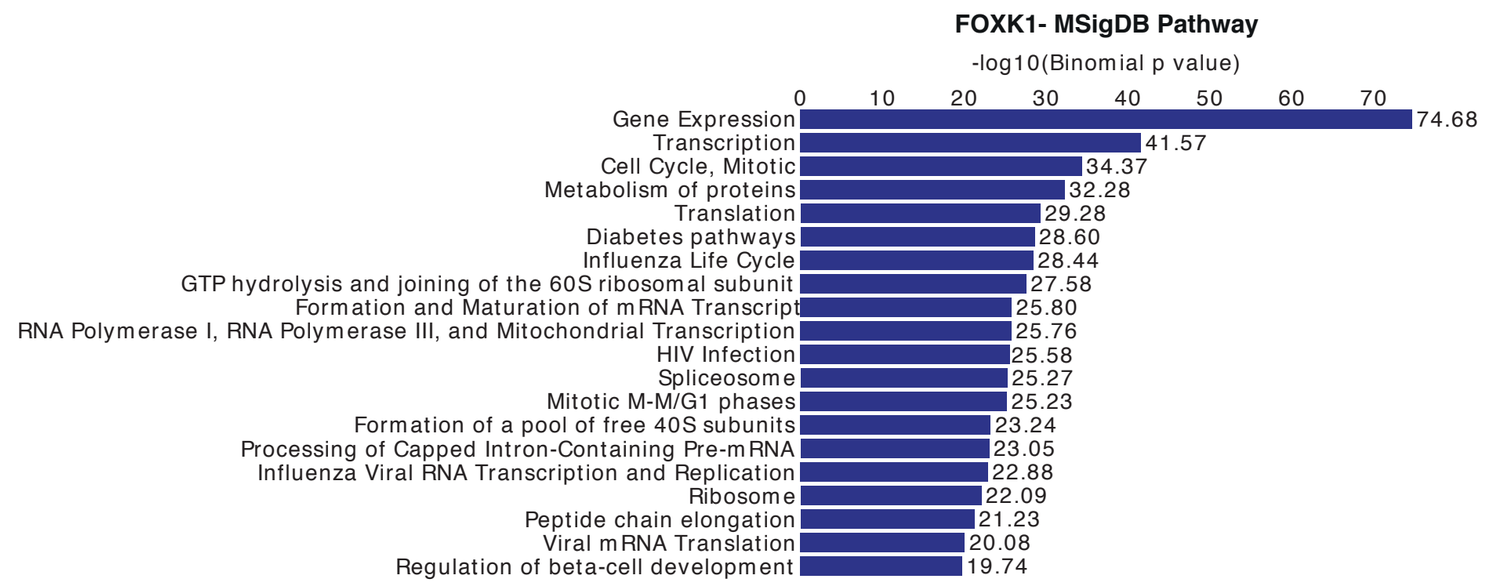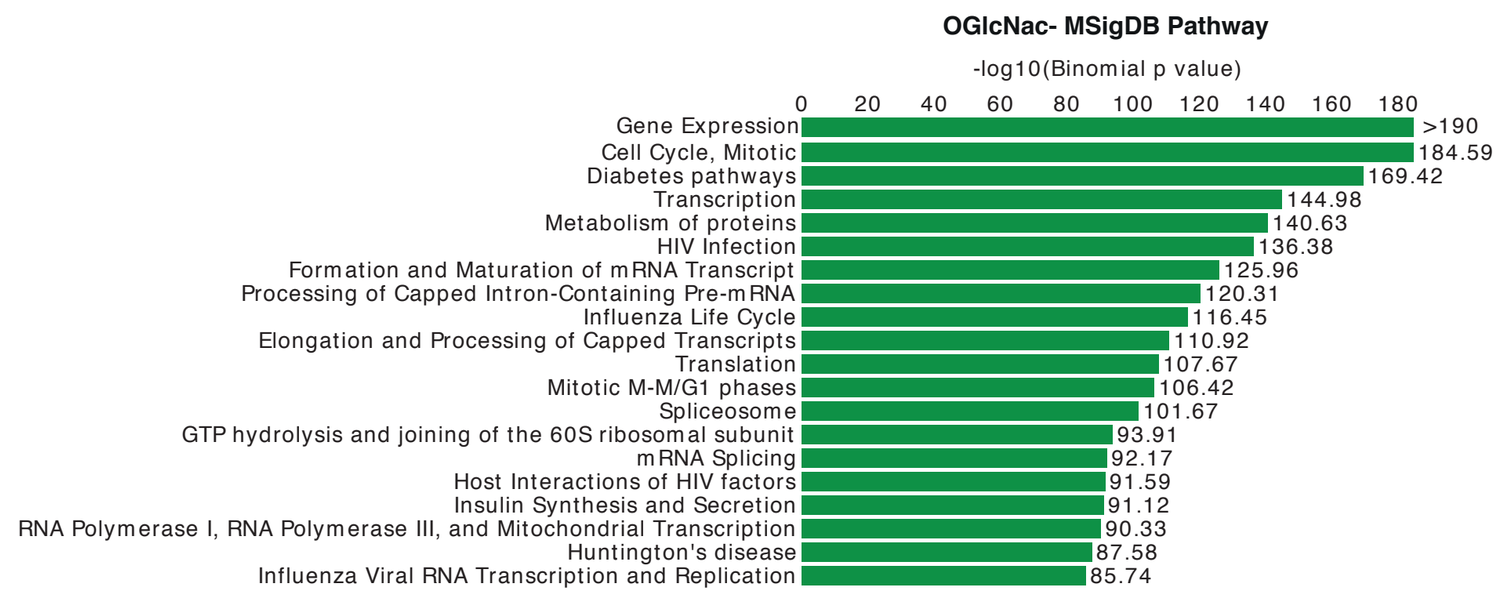
c